AD A091978

DTIC ELECTE II

DNA 5155F

CALCULATION OF MULTIPLE BURST INTERACTIONS FOR SIX SIMULTANEOUS EXPLOSIONS OF 120 TON ANFO CHARGES

Kaman AviDyne
83 Second Avenue
Burlington, Massachusetts 01803

15 December 1979

Final Report for Period 1 March 1979—15 December 1979

CONTRACT No. DNA 001-79-C-0224

APPROVED FOR PUBLIC RELEASE;
DISTRIBUTION UNLIMITED.

DTIC
ELECTE
NOV 2 4 1980

THIS WORK SPONSORED BY THE DEFENSE NUCLEAR AGENCY
UNDER RDT&E RMSS CODE B344079464 Y99QAXSG67704 H2590D.

DDC FILE COPY

Prepared for
Director
DEFENSE NUCLEAR AGENCY
Washington, D. C. 20305

80 11 21 055

Destroy this report when it is no longer needed. Do not return to sender.

PLEASE NOTIFY THE DEFENSE NUCLEAR AGENCY, ATTN: STTI, WASHINGTON, D.C. 20305, IF YOUR ADDRESS IS INCORRECT, IF YOU WISH TO BE DELETED FROM THE DISTRIBUTION LIST, OR IF THE ADDRESSEE IS NO LONGER EMPLOYED BY YOUR ORGANIZATION.

UNCLASSIFIED

SECURITY CLASSIFICATION OF THIS PAGE (When Data Entered)

REPORT DOCUMENTATION PAGE

READ INSTRUCTIONS BEFORE COMPLETING FORM

1. REPORT NUMBER	2. GOVT ACCESSION NO.	3. RECIPIENT'S CATALOG NUMBER
DNA 5155F	AD-A091978	

4. TITLE (and Subtitle)

CALCULATION OF MULTIPLE BURST INTERACTIONS FOR SIX SIMULTANEOUS EXPLOSIONS OF 12 TON ANFO CHARGES.

5. TYPE OF REPORT & PERIOD COVERED

Final Report for Period 1 Mar 79—15 Dec 79

6. PERFORMING ORG. REPORT NUMBER

KA-TR-176

7. AUTHOR(s)

J. R. Ruetenik
P. H. Hobbs
F. Smiley

8. CONTRACT OR GRANT NUMBER(s)

DNA001-79-C-0224

9. PERFORMING ORGANIZATION NAME AND ADDRESS

Kaman AviDyne
83 Second Avenue
Burlington, Massachusetts 01803

10. PROGRAM ELEMENT, PROJECT, TASK AREA & WORK UNIT NUMBERS

Subtask Y99QAXSG677-04

11. CONTROLLING OFFICE NAME AND ADDRESS

Director
Defense Nuclear Agency
Washington, DC 20305

12. REPORT DATE

15 December 1979

13. NUMBER OF PAGES

60

14. MONITORING AGENCY NAME & ADDRESS (if different from Controlling Office)

G-6 17

12 61

15. SECURITY CLASS. (of this report)

UNCLASSIFIED

15a. DECLASSIFICATION DOWNGRADING SCHEDULE

16. DISTRIBUTION STATEMENT (of this Report)

Approved for public release; distribution unlimited.

17. DISTRIBUTION STATEMENT (of the abstract entered in Block 20, if different from Report)

18. SUPPLEMENTARY NOTES

This work sponsored by the Defense Nuclear Agency under RDT&E RMSS Code B344079464 Y99QAXSG67704 H2590D.

19. KEY WORDS (Continue on reverse side if necessary and identify by block number)

Blast
Computer Studies
Pressure
Shock

20. ABSTRACT (Continue on reverse side if necessary and identify by block number)

The REFLECT code was modified for calculation of the interaction of six equal blast waves from simultaneously detonated charges in a hexagonal pattern. The objective has been to determine whether the REFLECT code, if further modified, would have the potential for accurate calculation of the interaction of six blast waves. In its present form the code is called REFLECT-3.

DD FORM 1 JAN 73 1473 EDITION OF 1 NOV 65 IS OBSOLETE

UNCLASSIFIED

SECURITY CLASSIFICATION OF THIS PAGE (When Data Entered)

194970

20. ABSTRACT (Continued)

A calculation was performed for the conditions of the MISERS BLUFF II-2 test, six 120-T ANFO charges separated by 100 m. Comparisons with overpressure and shock arrival time measurements show good agreement, within the data uncertainty, until the incident shock is within about 7 m (20 feet) of the array center. The peak overpressure predicted for the main reflected wave, which contains the highest pressures, agrees well with test results near the array center. Improvement would require reducing the cell sizes and applying the "sharp" (Rankine-Hugoniot) shock modelling not just to the initial shock but to two later shocks as well.

Accession For
NTIS GRA&I
DTIC TAB
Unannounced
Justification
By
Distribution/
Availability Codes
Dist | Special
A

Conversion factors for U.S. customary to metric (SI) units of measurement.

To Convert From	To	Multiply By
angstrom	meters (m)	1.000 000 X E -10
atmosphere (normal)	kilo pascal (kPa)	1.013 25 X E +2
bar	kilo pascal (kPa)	1.000 000 X E +2
barn	meter^2 (m^2)	1.000 000 X E -28
British thermal unit (thermochemical)	joule (J)	1.054 350 X E +3
calorie (thermochemical)	joule (J)	4.184 000
cal (thermochemical)/cm^2	mega joule/m^2 (MJ/m^2)	4.184 000 X E -2
curie	giga becquerel (GBq)*	3.700 000 X E +1
degree (angle)	radian (rad)	1.745 329 X E -2
degree Fahrenheit	degree kelvin (K)	t_k = (t° f + 459.67)/1.8
electron volt	joule (J)	1.602 19 X E -19
erg	joule (J)	1.000 000 X E -7
erg/second	watt (W)	1.000 000 X E -7
foot	meter (m)	3.048 000 X E -1
foot-pound-force	joule (J)	1.355 818
gallon (U.S. liquid)	meter^3 (m^3)	3.785 412 X E -3
inch	meter (m)	2.540 000 X E -2
jerk	joule (J)	1.000 000 X E +9
joule/kilogram (J/kg) (radiation dose absorbed)	Gray (Gy)**	1.000 000
kilotons	terajoules	4.184
kip (1000 lbf)	newton (N)	4.448 222 X E +3
kip/inch^2 (ksi)	kilo pascal (kPa)	6.894 757 X E +1
ktap	newton-second/m^2 ($N-s/m^2$)	1.000 000 X E +2
micron	meter (m)	1.000 000 X E -6
mil	meter (m)	2.540 000 X E -5
mile (international)	meter (m)	1.609 344 X E +3
ounce	kilogram (kg)	2.834 952 X E -2
pound-force (lbf avoirdupois)	newton (N)	4.448 222
pound-force inch	newton meter (N·m)	1.129 848 X E -1
pound-force/inch	newton/meter (N/m)	1.751 268 X E +2
pound-force/foot^2	kilo pascal (kPa)	4.788 026 X E -2
pound-force/inch^2 (psi)	kilo pascal (kPa)	6.894 757
pound-mass (lbm avoirdupois)	kilogram (kg)	4.535 924 X E -1
pound-mass-foot^2 (moment of inertia)	kilogram-meter^2 ($kg·m^2$)	4.214 011 X E -2
pound-mass/foot^3	kilogram/meter^3 (kg/m^3)	1.601 846 X E +1
rad (radiation dose absorbed)	Gray (Gy)**	1.000 000 X E -2
roentgen	coulomb/kilogram (C/kg)	2.579 760 X E -4
shake	second (s)	1.000 000 X E -8
slug	kilogram (kg)	1.459 390 X E +1
torr (mm Hg, 0° C)	kilo pascal (kPa)	1.333 22 X E -1

*The becquerel (Bq) is the SI unit of radioactivity; 1 Bq = 1 event/s.
**The Gray (Gy) is the SI unit of absorbed radiation.

A more complete listing of conversions may be found in "Metric Practice Guide E 380-74," American Society for Testing and Materials.

PREFACE

The work described here was performed by the AviDyne Division of the Kaman Sciences Corporation for the Defense Nuclear Agency under Contract DNA001-79-C-0224. Dr. George W. Ullrich of the DNA Shock Physics Directorate was the technical monitor.

Dr. J. Ray Ruetenik of Kaman AviDyne was the project leader under Dr. Norman P. Hobbs, Technical Director of KA. Dr. Hobbs and Mr. Robert F. Smiley carried out the computer code work assisted by Messrs. Thomas A. Dalton and Michael A. Tomayko.

Appreciation is expressed to Dr. Ullrich for his interest and technical interchange during the progress of the work. Particular appreciation is extended to Dr. Allen L. Kuhl, R&D Associates, for his comments during the course of this work.

TABLE OF CONTENTS

LIST OF ILLUSTRATIONS

SECTION 1
INTRODUCTION

The interaction of blast waves from two or more simultaneous explosions can lead to much higher pressures than would be found from the individual blast waves. This phenomenon has been called cumulation by Kuhl (Reference 1) in a thorough analysis of the interaction for a six-burst situation described below.

A field test designated MISERS BLUFF II-2 (MB II-2) was conducted by the Defense Nuclear Agency at the Planet Ranch test site near Lake Havasu, Arizona, 30 August 1978, for measuring the interaction of six blast waves from the simultaneous detonation of six 120-ton ANFO charges arranged in a hexagonal pattern with 100-meter separation.

Reference 1 presents a comprehensive analysis of the basic interactions involved in this six-burst blast interaction. Reference 1 also develops a semi-empirical method for prediction of the peak shock overpressures and makes comparisons with the measured data from the MB II-2 test. The need for a hydrocode to be used in prediction of the interaction, particularly to obtain overpressure-time waveforms, is noted in Reference 1.

The objective of the present investigation has been to determine whether the REFLECT hydrocode would have the potential, if modified, for computing the interaction of blast waves from multiple nuclear bursts simultaneously detonated at ground level and to indicate the modifications needed.

A principal feature of the REFLECT code is the representation of the refracted (reflected) shock waves in a two-burst interaction as "sharp" shocks using the Rankine-Hugoniot (R-H) equations. If blast waves from additional bursts interact with these blast waves, as for the six-burst array being studied, it is expected that the additional shock waves might also have to be represented in such a calculation by the R-H equations in order to obtain satisfactory accuracy.

The approach taken has been to make a limited modification to the REFLECT code so that a preliminary comparison could be made of the code results with the MB II-2 test data. Only the two shock waves that are currently modelled in the code as R-H shocks, the first refracted shock and the first Mach shock, would be modelled. The shock waves appearing later would then be smeared shocks in these calculations. This comparison would enable an assessment to be made of the potential of the REFLECT code were one or more of the additional shock waves to be modelled as R-H shocks.

Sharp R-H shock representation is expected to be very important to accurate calculation of blast wave interaction from multiple bursts. Without R-H shock modelling, the shocks become smeared as compressions over a number of cells introducing strong numerical viscous effects into the computed interaction. Several other improvements to the REFLECT code should also be considered for the calculations, and they will be discussed and summarized below.

SECTION 2
REFLECT-3 HYDROCODE

2-1 REFLECT-1 MODEL FOR TWO-BURST INTERACTION.

The blast wave pattern for six charges in a hexagonal pattern is shown in Figure 1 for a time shortly after the waves begin to interact. The blast waves all first interact at the charge bisectors. Because the charges are equally spaced and equidistant from the array center, the wave pattern is symmetrical on the two sides of each of the six charge bicectors.

The REFLECT-1 code (Reference 2) computes the flow field within the shaded region for a plane of symmetry which is in this case the charge bisector plane. The solution is axisymmetric about the line joining the two charges. A sketch illustrating the REFLECT-1 solution and its relationship to the six-burst problem is shown in Figure 2. The code computes the flow field between the refracted blast shock and the charge bisector plane until the time that the refracted shock intercepts the plane of the charge radial.

The REFLECT code employs the Godunov differencing scheme (Reference 3) with an expanding cell system. The cell system, Figure 2, is axisymmetric about the axis passing through two adjacent burst centers. Each cell is a torus centered about the axis. The cells are arranged in columns with the generators for each column emanating from a common point on the axis on the opposite side of the charge bisector plane.

The refracted blast shock R_1 is one boundary of the cell system. The charge bisector plane is the second boundary of the cell system. After the Mach shock M_1 forms between the intersection of the shocks I_1 and R_1 and the bisector, it becomes the third boundary of the cell system. Further description of the cell system is given in Reference 2.

The Godunov method conserves mass, momentum and energy in each cell. The equation of state for air is taken from Brode (Reference 4).

The REFLECT-1 code then computes the flow within the region in Figure 2 bounded by the refracted shock R_1, the charge bisector plane and the Mach shock M_1 after it forms, Figure 3. The boundary conditions for the calculation are the following. At the shock R_1 the properties and flow velocities of the blast wave immediately outside of the shock provide the boundary conditions. At the bisector plane the impermeable surface conditions apply. At the Mach shock M_1, when it forms, the atmospheric conditions apply at the boundary.

The cell layout used in the present calculations is the same layout employed in Reference 2. There are 24 columns of cells between the axis and the triangular corner cell at the juncture of the R_1 wave

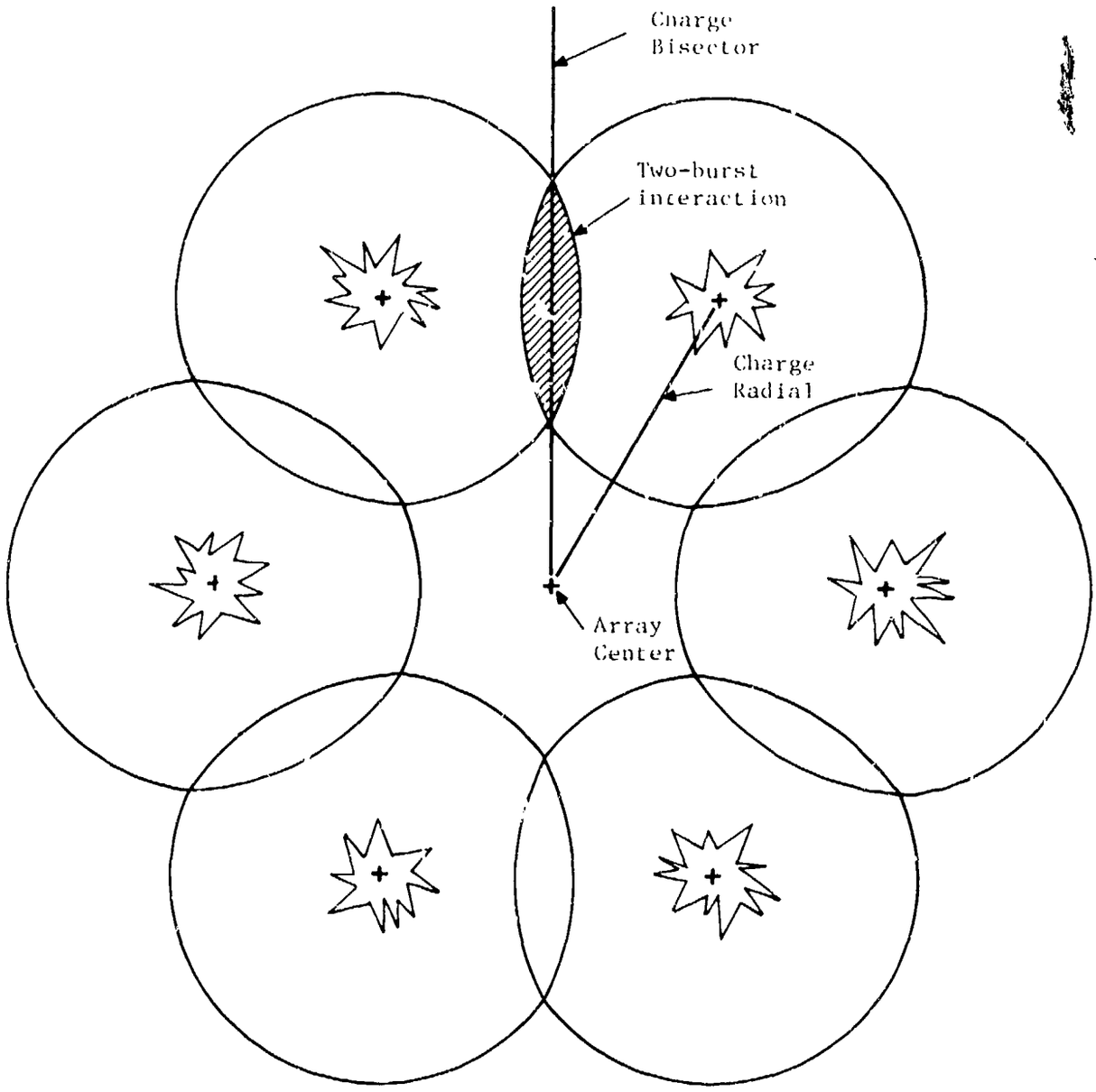

Figure 1. Blast pattern shortly following simultaneous burst of a hexagonal array of charges.

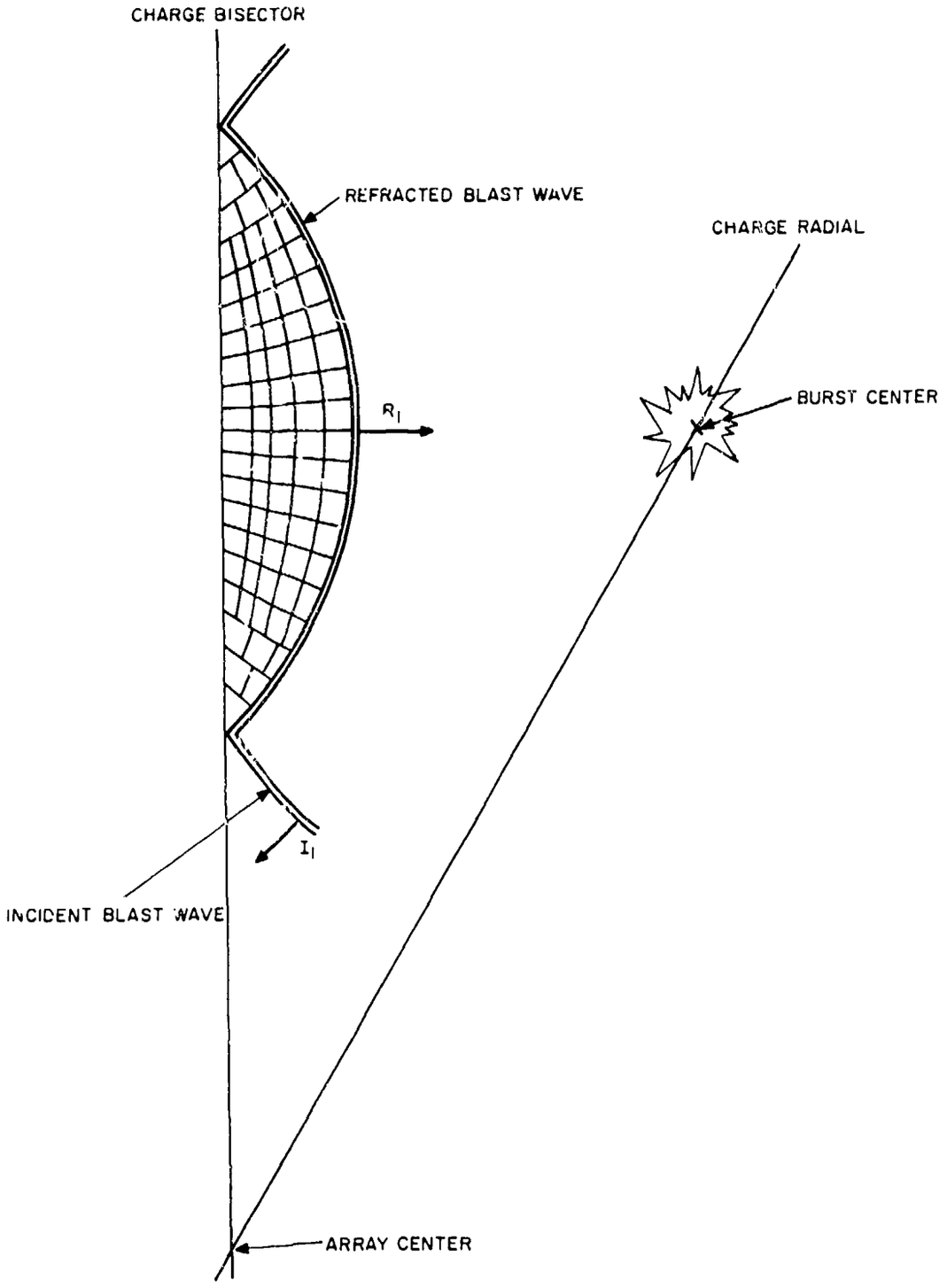

Figure 2. REFLECT-1 model of two-burst blast interaction.

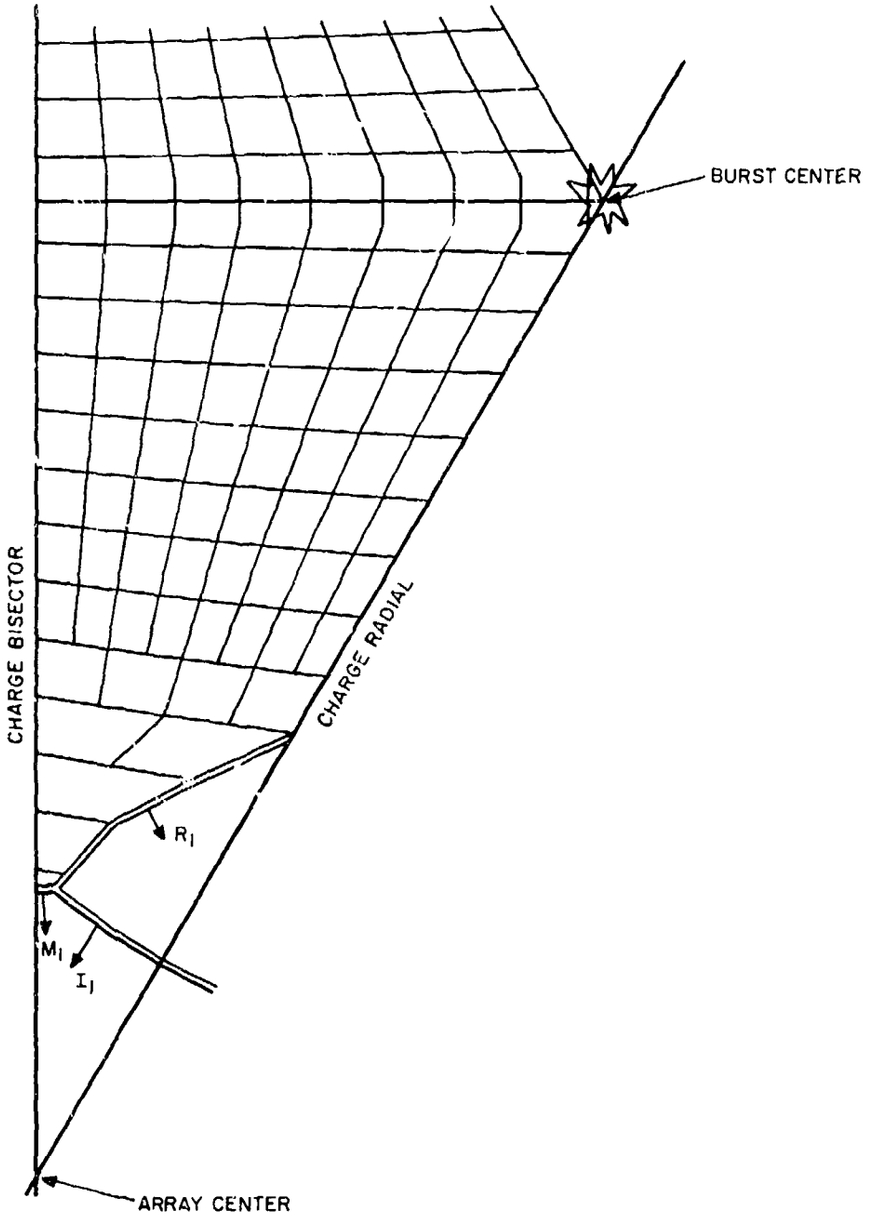

Figure 3. REFLECT-3 cell layout after R_1 wave intercepts charge radial.

with the charge bisector. The number of cells in a column decreases stepwise from the axis to the corner cell. Also, the number of cells within a column increases with time as the cell system expands. The maximum number of cells in a column is limited to 16.

After the Mach shock M_1 is formed the triangular corner cell is replaced by one or more four-sided cells. This cell array is called the outer mesh system in Reference 2. The maximum number of cells reached in the outer mesh system in the present calculations was 16 in a 4 x 4 array.

The number of cells used in the present calculations was limited to the capability of the REFLECT code developed in Reference 2. A recommended improvement to be emphasized below would be to increase the number of cells significantly.

2-2 SIX-BURST INTERACTION.

Up to the point in the calculation where the shock R_1 reaches the charge radial the REFLECT-3 code is the same as the REFLECT-1 code of Reference 2, with the exception of improvements made to the code regarding iteration methods, tolerances and other associated techniques.

When the R_1 shock reaches the charge radial the changes made for the REFLECT-3 code apply. The cell layout for this period is shown in Figure 3, where each cell shown in the sketch represents four cells in the calculation.

The adaptation made to the REFLECT-1 code for this problem has been to limit the expansion of the cell system to the boundary provided by the charge radial. Therefore each column of cell cross-sections shown in Figure 2 expands until it reaches the charge radial, as shown in Figure 3. In the inner nine columns shown in the sketch the cells are bounded by the charge radial. The outer four columns are bounded by the reflected shock R_1 and the Mach shock M_1. As the incident shock I_1 moves closer to the array center, the remaining columns one by one reach the charge radial. During the whole period, of course, the width of the columns increases.

When the cells reach the charge radial, a pressure wave reflects back towards the charge bisector. This is the refracted shock wave from the next clockwise burst, 90 degrees from the bisector.

The sequence of waves from the time the blast waves first interact is shown in Figure 4. The waves are sketched in this figure essentially in the shape obtained in the REFLECT-3 results. The shock waves that are computed correctly as R-H shocks are identified by double lines and the other shocks by single lines.

Adjacent blast waves first interact on the charge bisectors at 284.1 feet from the array center, Figure 4a. The shock pattern after the initial interaction is shown in Figure 4b. Up to this point all the shock waves are computed by the REFLECT-3 code as R-H shocks.

The pattern after the Mach shock M_1 forms is shown in Figure 4c. The refracted shock R_2 is not represented as an R-H shock in the REFLECT-3 code, so it smears over several cells. The results of the REFLECT-3 calculations indicate the triple point I_1-R_1-M_1 intercepts the charge radial at 24.5 feet from the array center. This compares well with the 24 feet given by the method of Kuhl (Reference 1).

After the triple point I_1-R_1-M_1 intercepts the charge radial, the Mach shock M_2 is formed with the triple point M_1-R_2-M_2. Because the shock R_2 is smeared in the present form of the REFLECT-3 code, the triple point becomes spread out along the incident shock M_1-M_2. The smeared triple point therefore would be expected to reach the charge bisector ahead of the time it would if instead it were formed by an R_2 shock that is sharp.

The arrival of the principal part of the smeared triple point was identified from the REFLECT-1 results by the abrupt rise in pressure behind the M_1 shock as being at 9 feet. This compares well with the arrival of the triple point given by Reference 1 as 8 feet.

The shock R_2 refracts across the charge bisector as the R_3 wave shown in Figure 4e and the Mach shock M_3 is formed. The shock R_3 is smeared in the REFLECT-3 calculations, but the front of the imploding wave continues to be formed by the R-H shock in the code. This imploding shock has the triple point M_2-R_3-M_3 according to the model of Reference 1.

The triple point M_2-R_3-M_3 is smeared in the calculations because the shock R_3 is smeared. The arrival of the leading edge of the smeared zone at the charge radial is indicated in the computed results by a marked rise in pressure behind shock M_2 at the radial at 3 feet from the array center. From there inward the results indicated that the pressure on the radial behind the incident shock increased to essentially equal the pressure at the bisector.

The REFLECT-3 calculations were continued until the incident shock on the bisector reached within 0.43 feet of the array center. At that point the cell system was frozen. From then on the waves moved through the mesh with all the waves being smeared. At this point the cell system had four cells along the imploding shock between the charge bisector and charge radial. Each cell had a 0.056-ft front on the imploding shock and a length in the radial direction of 0.20 feet.

The calculations were continued until 0.073 seconds after the scaled AFWL 1-KT-STD(REV) burst. This corresponds to about 0.080 seconds for the 120-ton ANFO bursts.

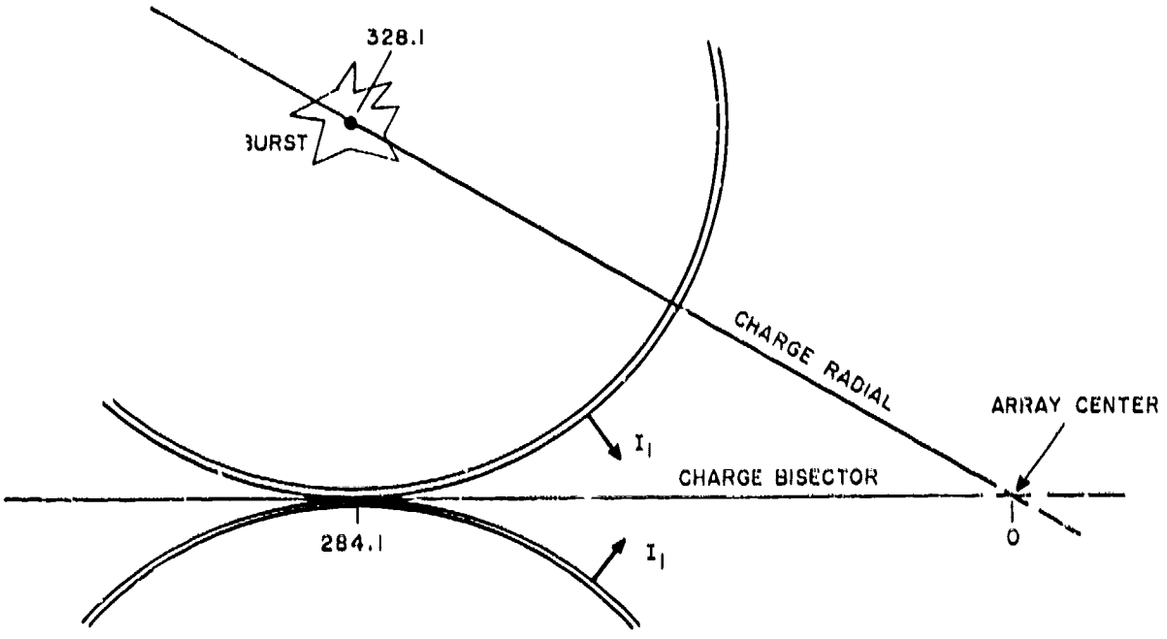

a. At two-burst intercept.

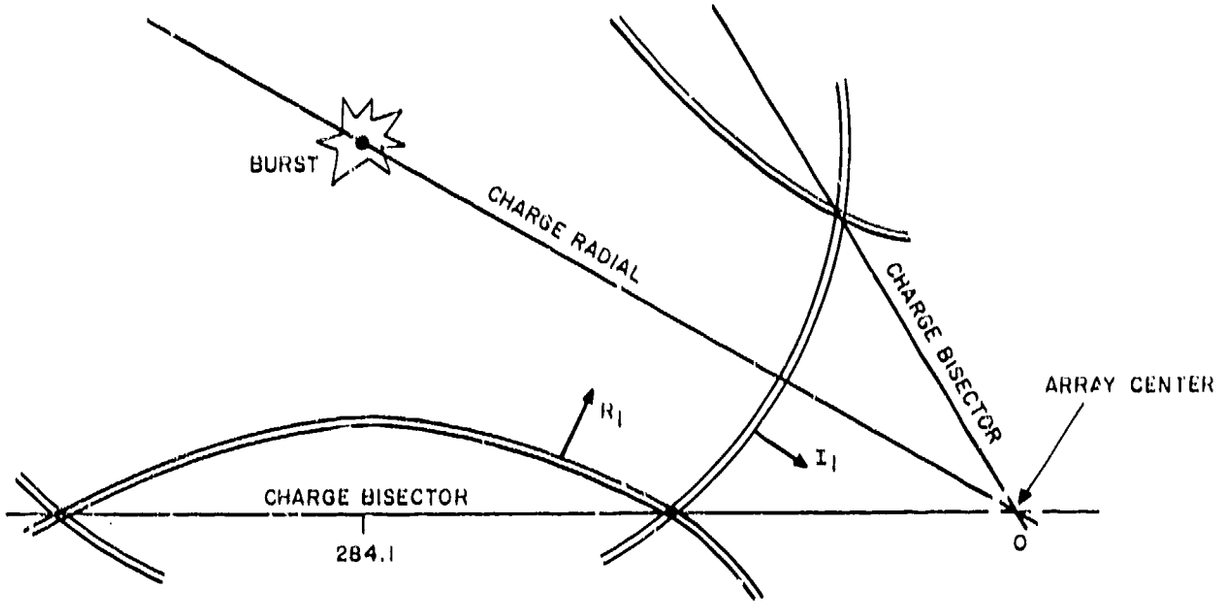

b. During two-burst regular shock interaction.

Figure 4. Sketches illustrating development of shock patterns.

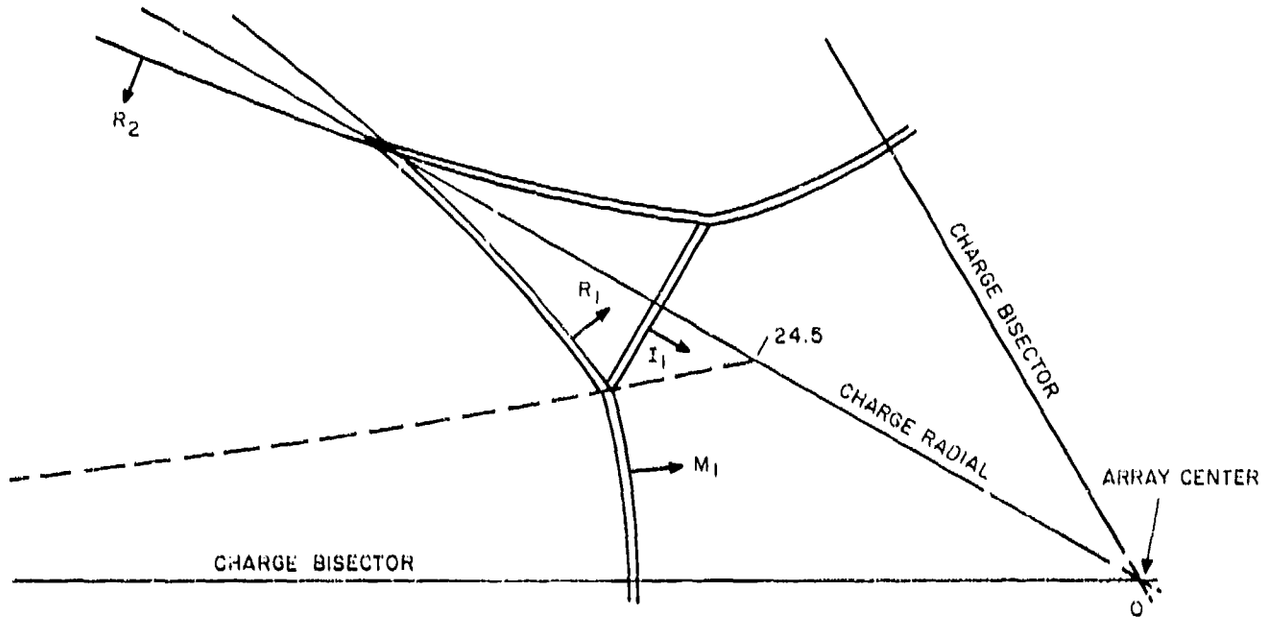

c. Before triple point I_1-R_1-M_1 reaches charge radial.

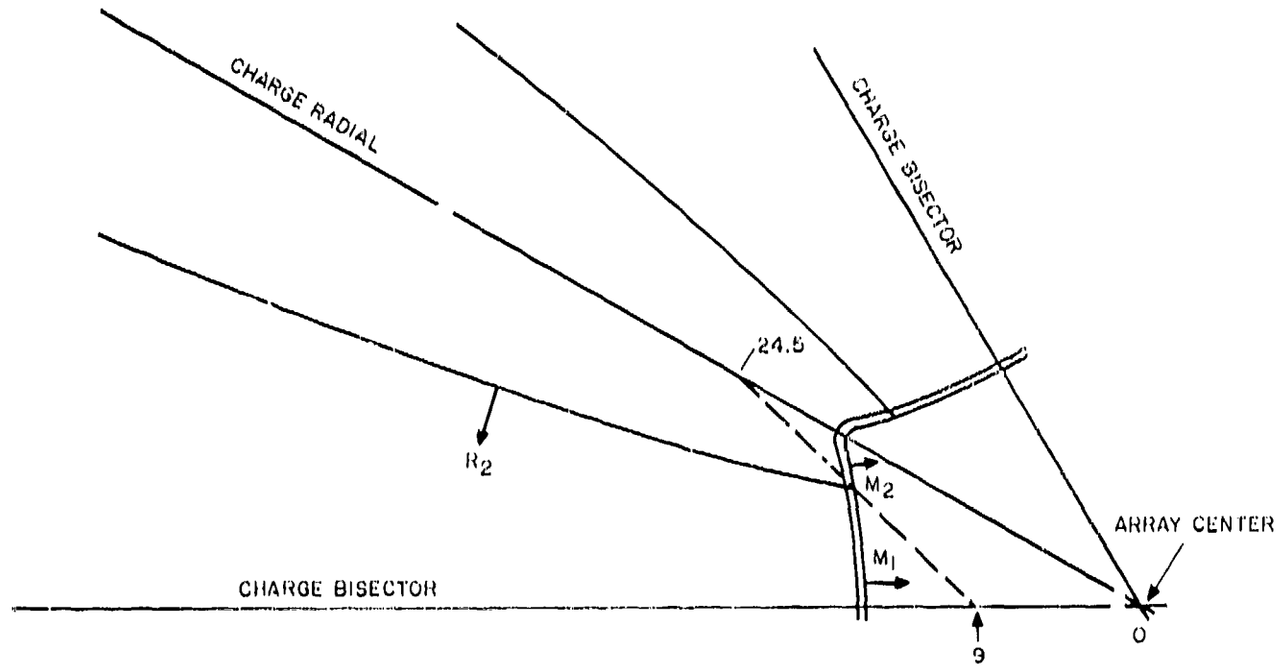

d. Triple point M_1-R_2-M_2 between charge radial and bisector.

Figure 4. (Continued)

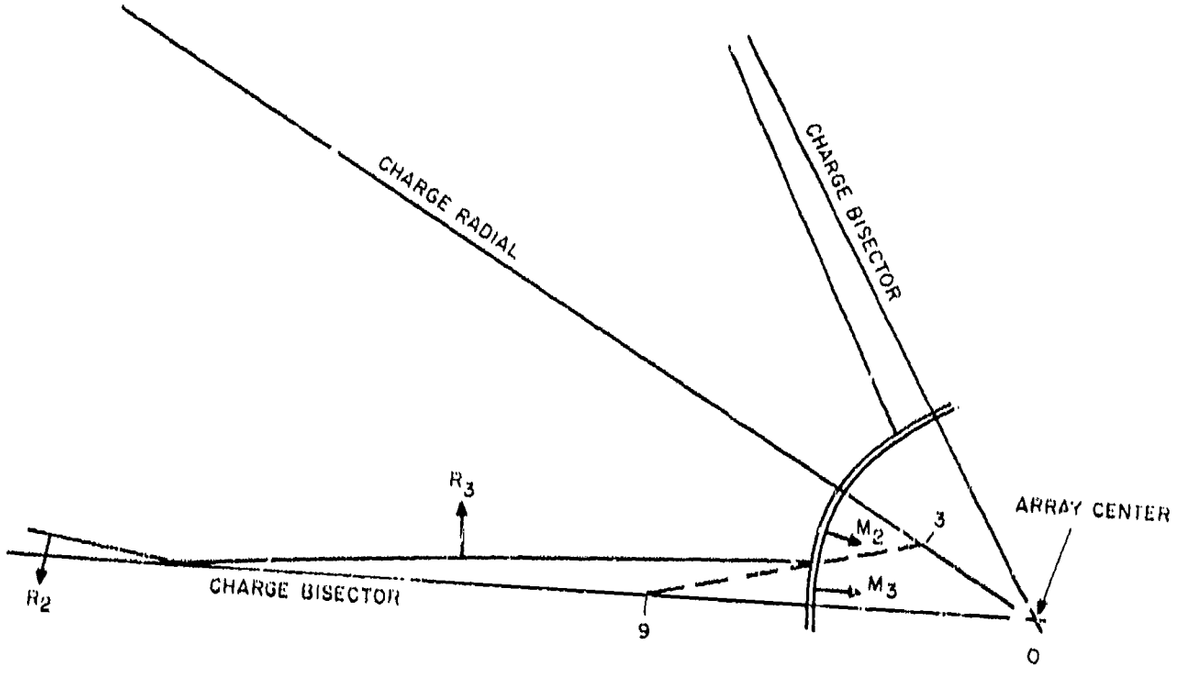

e. Triple point M_2-R_3-M_3 between charge bisector and radial.

Figure 4. (Concluded)

The PFAB code has been developed for computing the shock wave that radiates from the array center after the imploding wave r:aches the center. (This wave is called the main reflected wave in Reference 1). This code is described in the Appendix. The code computes the region inside of the outward-facing shock and the sector bounded by the charge bisector and radial. The boundary conditions for this zone are the conditions ahead of the outward-facing shock, given by the REFLECT-3 calculations, and the impermeable surface conditions at the charge bisector and radial. The PFAB code for computing this region has been prepared and debugged.

A computer routine is required to input the necessary data from the REFLECT-3 code into the PFAB code. The REFRA mating code was developed for use with the REFLECT-1 code output, and minor modifications are required for its use with the REFLECT-3 output.

There is a point concerning the three-dimensionality of the REFLECT-3 model that should be noted. The vertical plane from the ground along the charge radial is represented in the REFLECT-3 code as a slightly curved surface. This is due to the fact that the cell geometry of the REFLECT-3 code is axisymmetric about the axis joining the charges. In the code the boundary for the charge radial is a conical surface having its apex at the charge. The charge radial on the ground is a generatrix of the cone. The included angle of the cone is 120 degrees, so the radius of curvature normal to the surface is very large compared with the distance from the radial to the bisector, and the ratio of the two becomes infinite approaching the array center. Because the radius of curvature becomes increasingly large relative to the distance between the charge radial and charge bisector as the incident shock approaches the charge center, calculations have indicated that the curvature is not expected to have a significant influence on the results, particularly approaching the array center.

SECTION 3
RESULTS

The test results of the MISERS BLUFF II-2 test are presented in Figures 5 to 12. These results have been photocopied from Reference 1.

The free-air blast data are an input to the REFLECT-3 code. Two blast models are compared with the test data in Figures 5 and 6.

The records of the overpressures measured in the MB II-2 test are presented in Figures 6 and 7 for stations along the charge radials and bisectors, respectively. The records have been reproduced from Reference 1. The stations are identified by the radial distance from the array center in meters and angle from one of the charge bisectors in degrees; e.g., Station 25-30 is 25 meters from the array center and 30 degrees from the baseline charge bisector.

The output of the REFLECT-3 calculations is compared with the test results in Figures 6 and 7 for the charge radials and bisectors, respectively. The times for the REFLECT-3 results presented in these two figures have been adjusted to match the measured arrival of the first shock of each pressure record. The incident shock pressure-range results are compared with the test data in Figure 8. The pressure-range results for the main reflected wave are compared with the test data in Figures 9 and 10. The shock positions as a function of time are compared with the test results in Figures 11 and 12.

3-1 BLAST-WAVE MODEL.

3-1.1 Shock Overpressure.

The REFLECT code uses the data from the undisturbed blast wave from a single burst as input to the code calculations. The calculations are as accurate as this input.

The incident shock overpressure, Δp_s, given by two methods is compared in Figure 5 with data from the MB II-2 test results. The MB II-2 data used here for comparisons have been obtained from Reference 1. The abscissa is the distance from the center of the 6-burst array.

The crosses in Figure 5 represent the ANFO calculation by AFWL for the MB II-2 test as given in Reference 5. The shock overpressure presented here for these data was determined by the current method recommended by Reference 6 wherein the shock overpressure is taken as the peak computed pressure and the location of the shock is taken as the point where the computed pressure is one-half of the peak pressure. Previously Reference 7 had recommended a 4-point extrapolation of the pressures to obtain the shock overpressure. That method generally gives a shock overpressure about 2 to 4 percent higher than for the curve shown. At the 82-ft station the ANFO calculation gives a shock overpressure that is 10 percent higher than a mean of the data. For the 41-ft station the ANFO calculation shows good agreement with the test data.

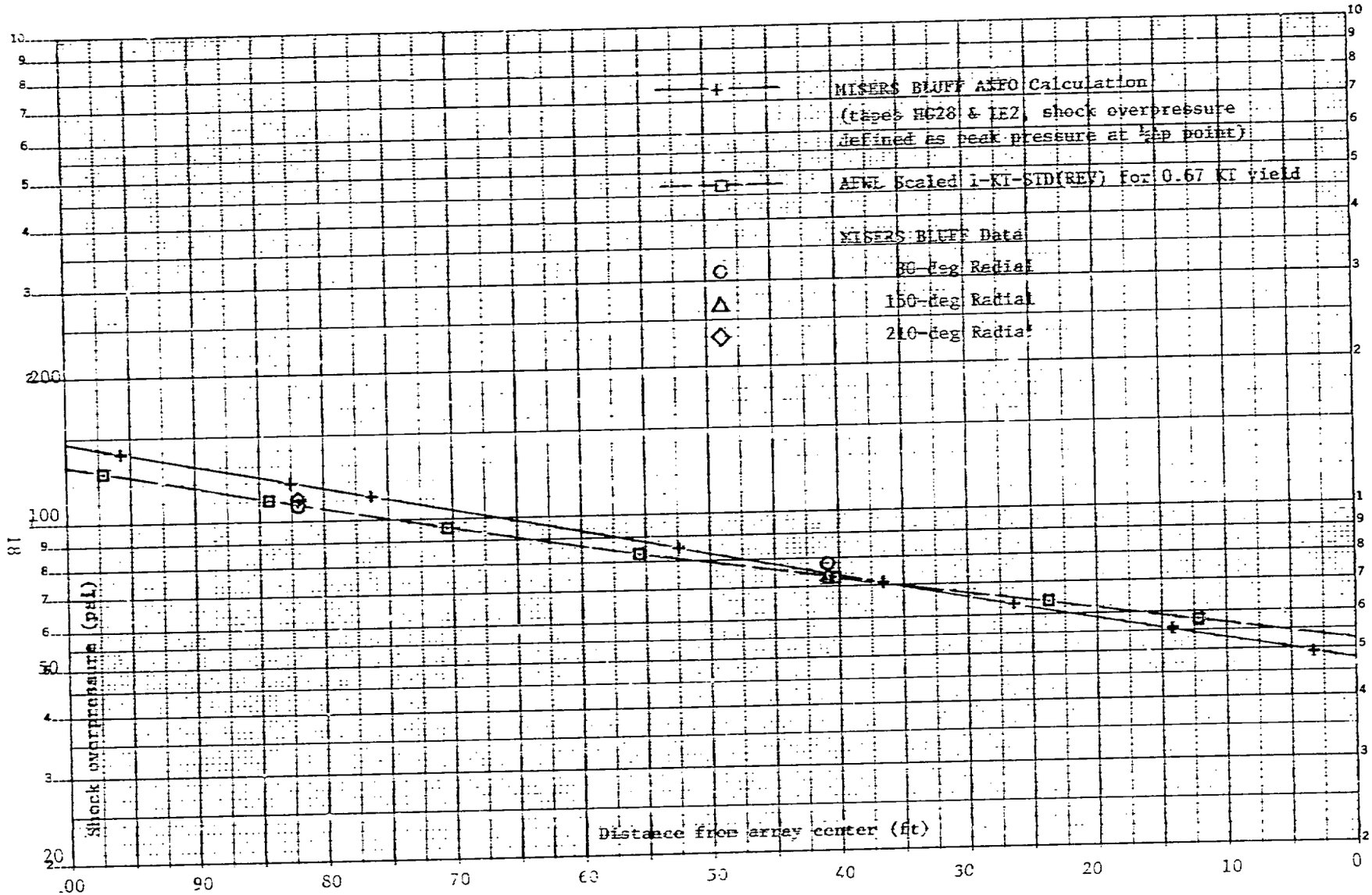

Figure 5. Comparison of predicted and measured shock overpressures for individual ANFO blast waves.

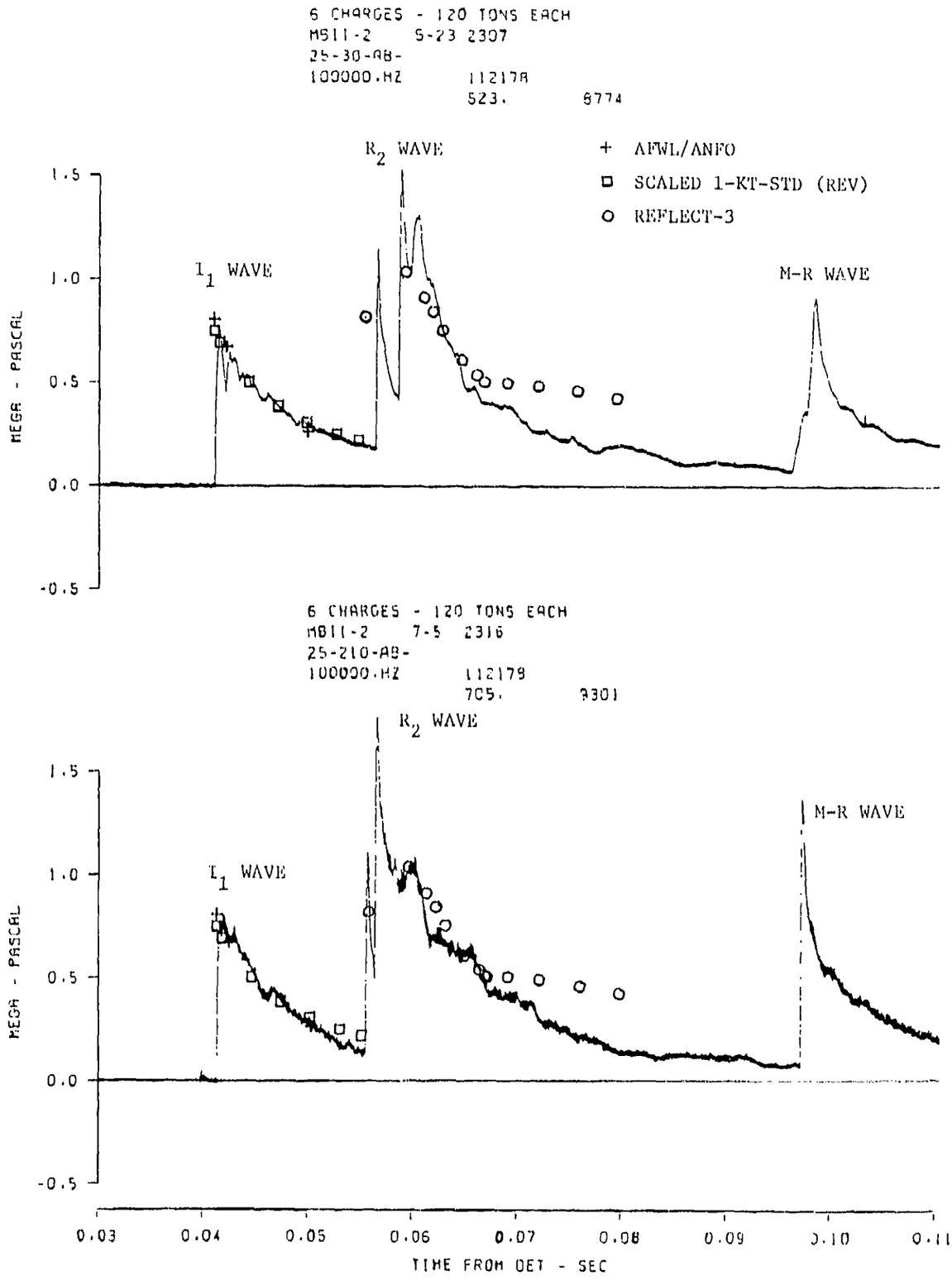

a. 82 feet from array center.

Figure 6. Comparison of overpressure predictions with MISERS BLUFF II-2 test data for charge locations. Traces represent test data.

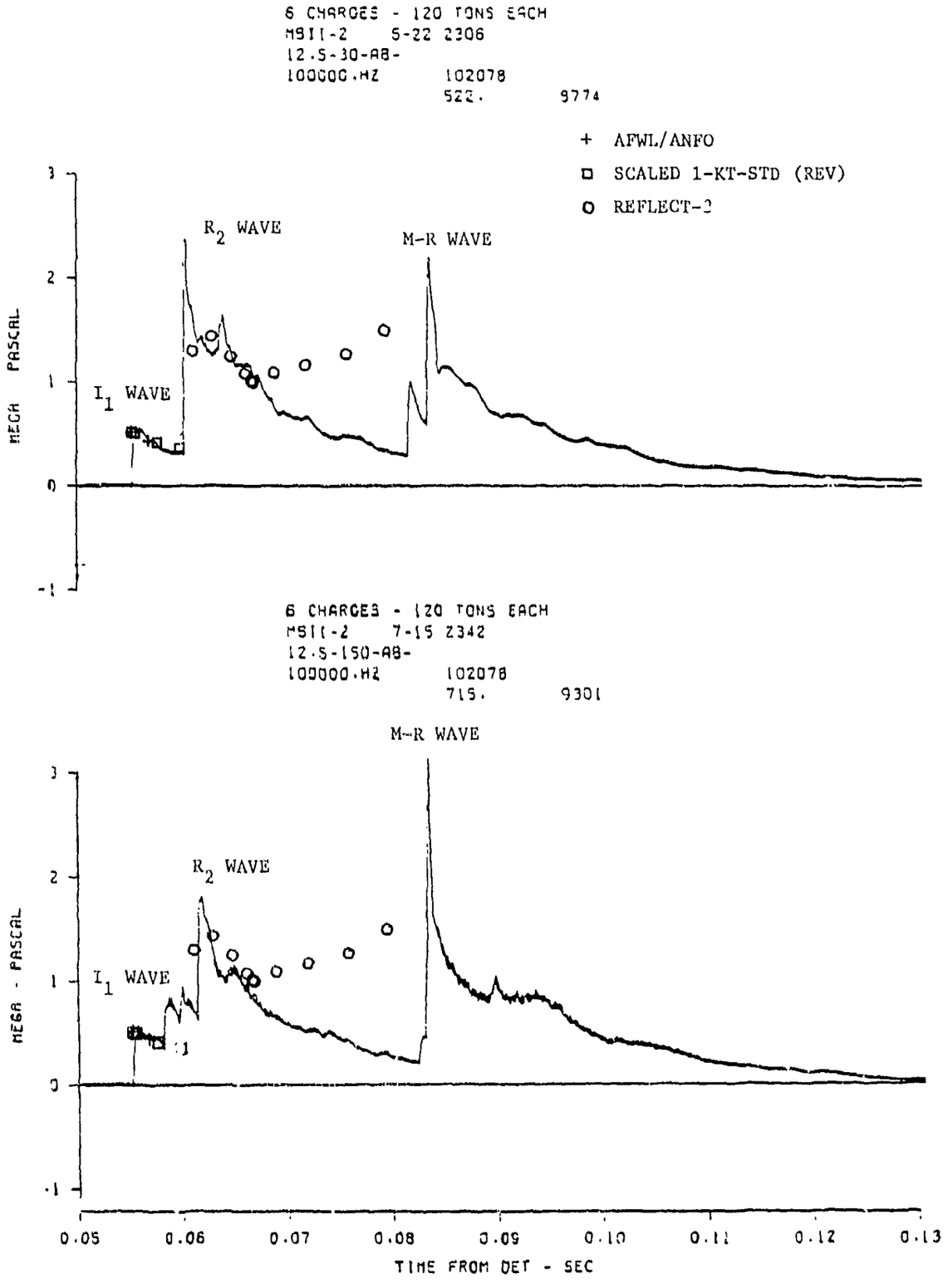

b. 41 feet from array center.

Figure 6. (Continued)

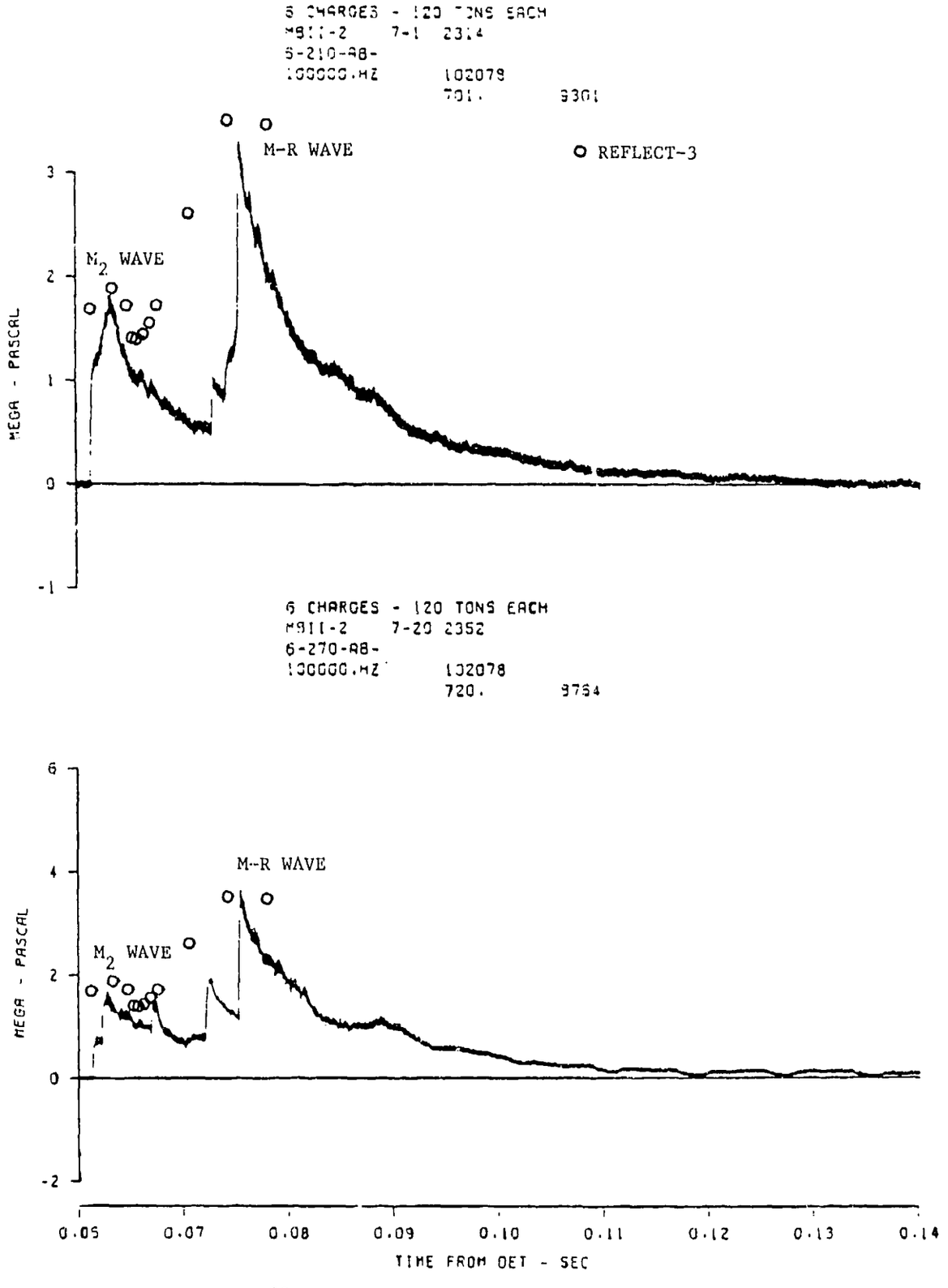

c. 20 feet from array center.

Figure 6. (Concluded)

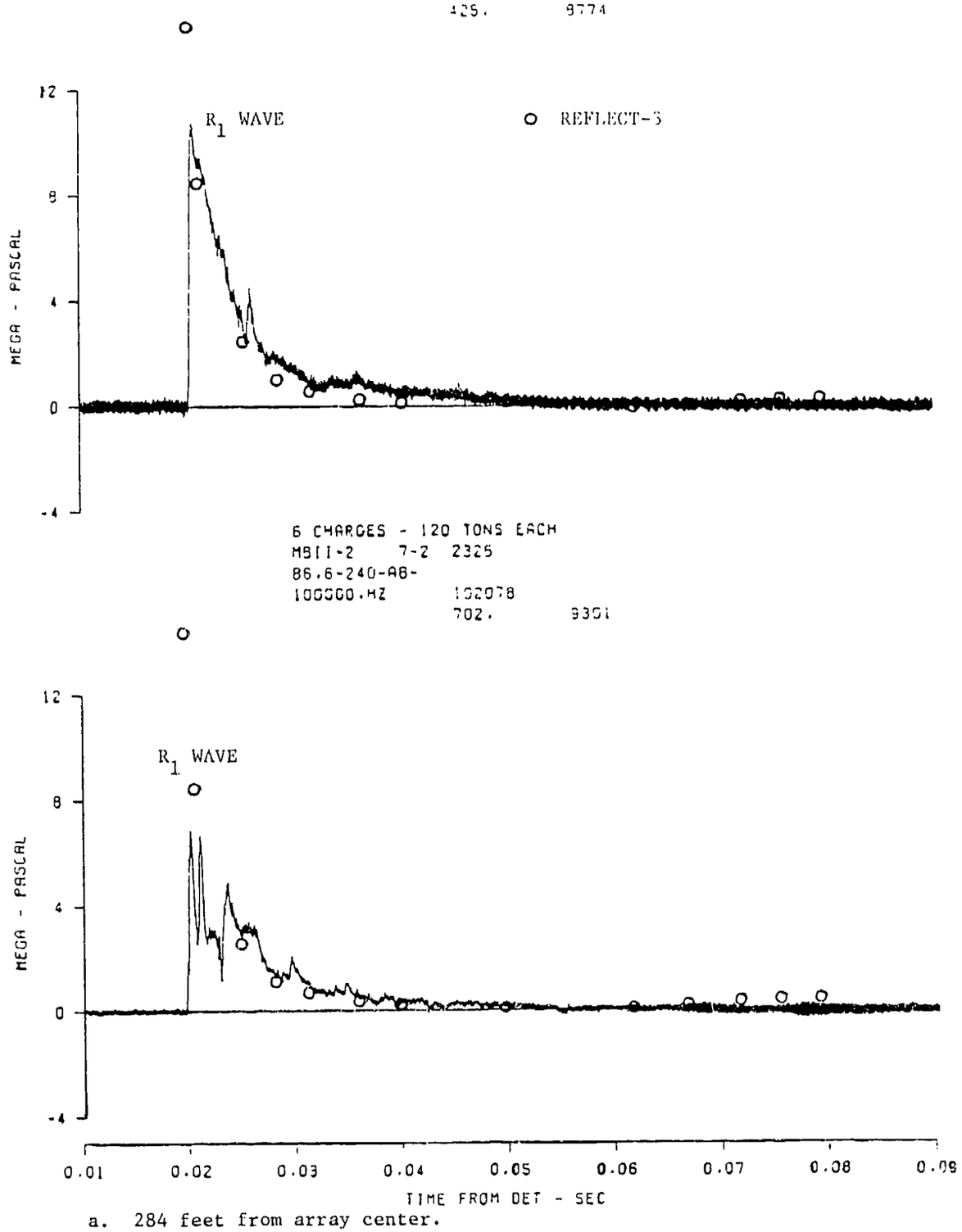

a. 284 feet from array center.

Figure 7. Comparison of overpressure predictions with MISERS BLUFF II-2 test data for charge bisector locations. Traces represent test data.

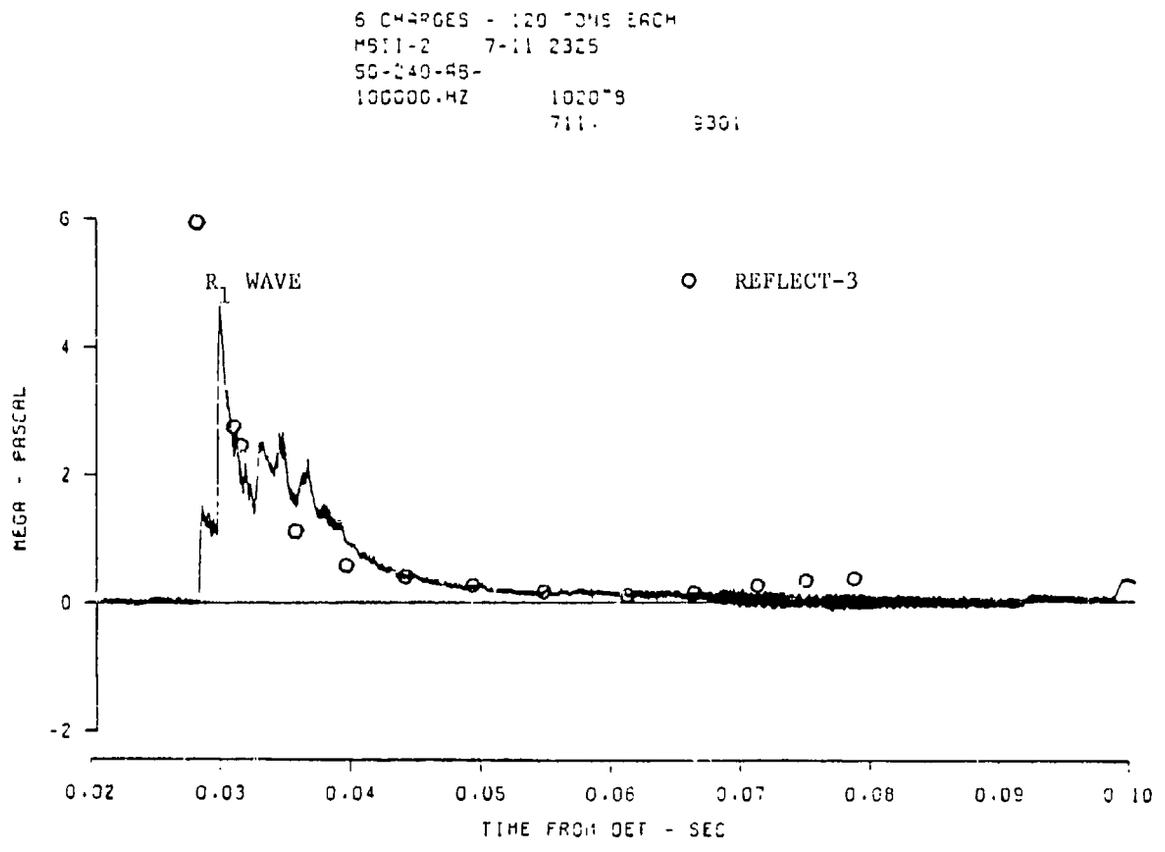

b. 164 feet from array center.

Figure 7. (Continued)

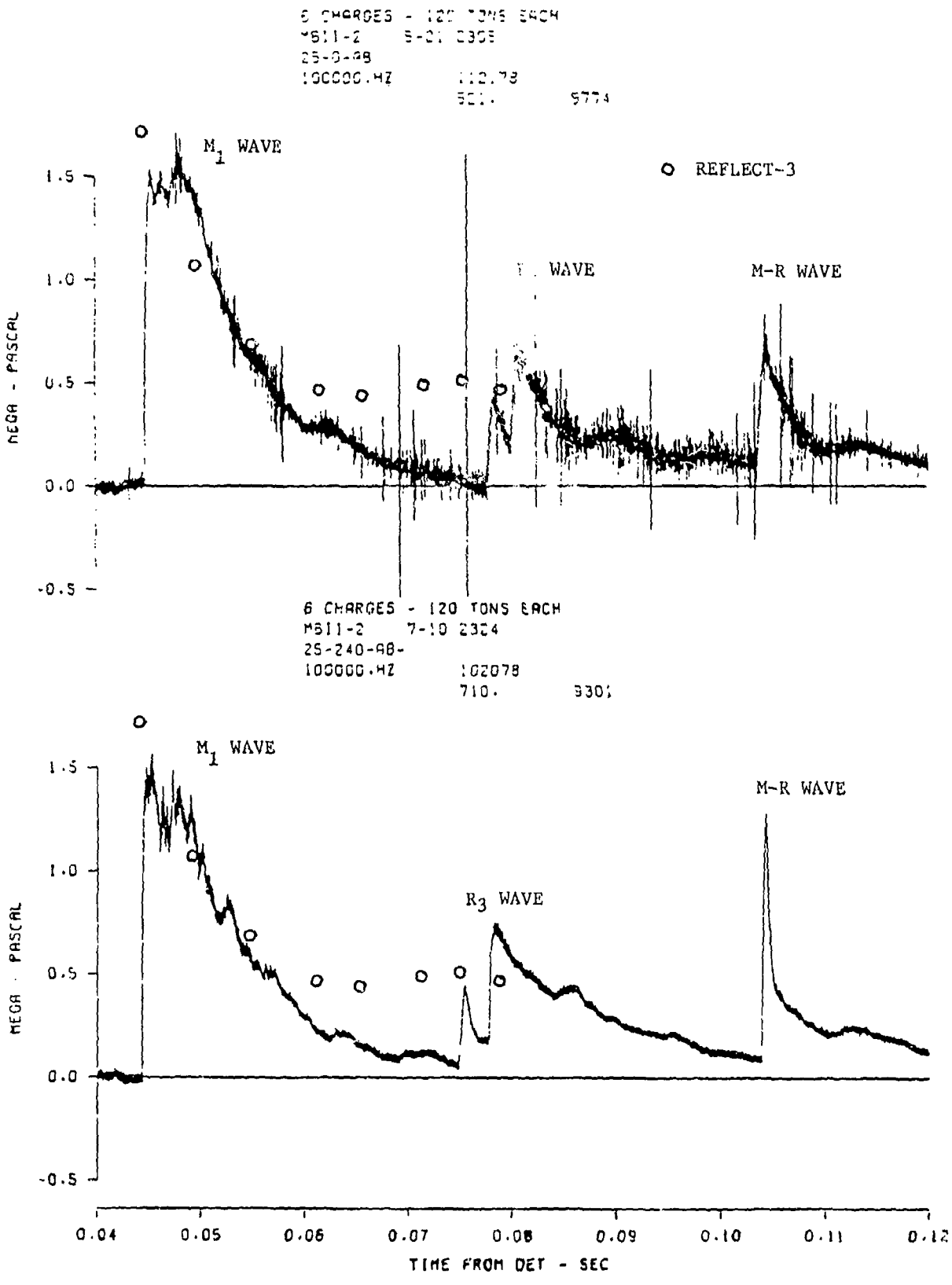

c. 82 feet from array center.

Figure 7. (Continued)

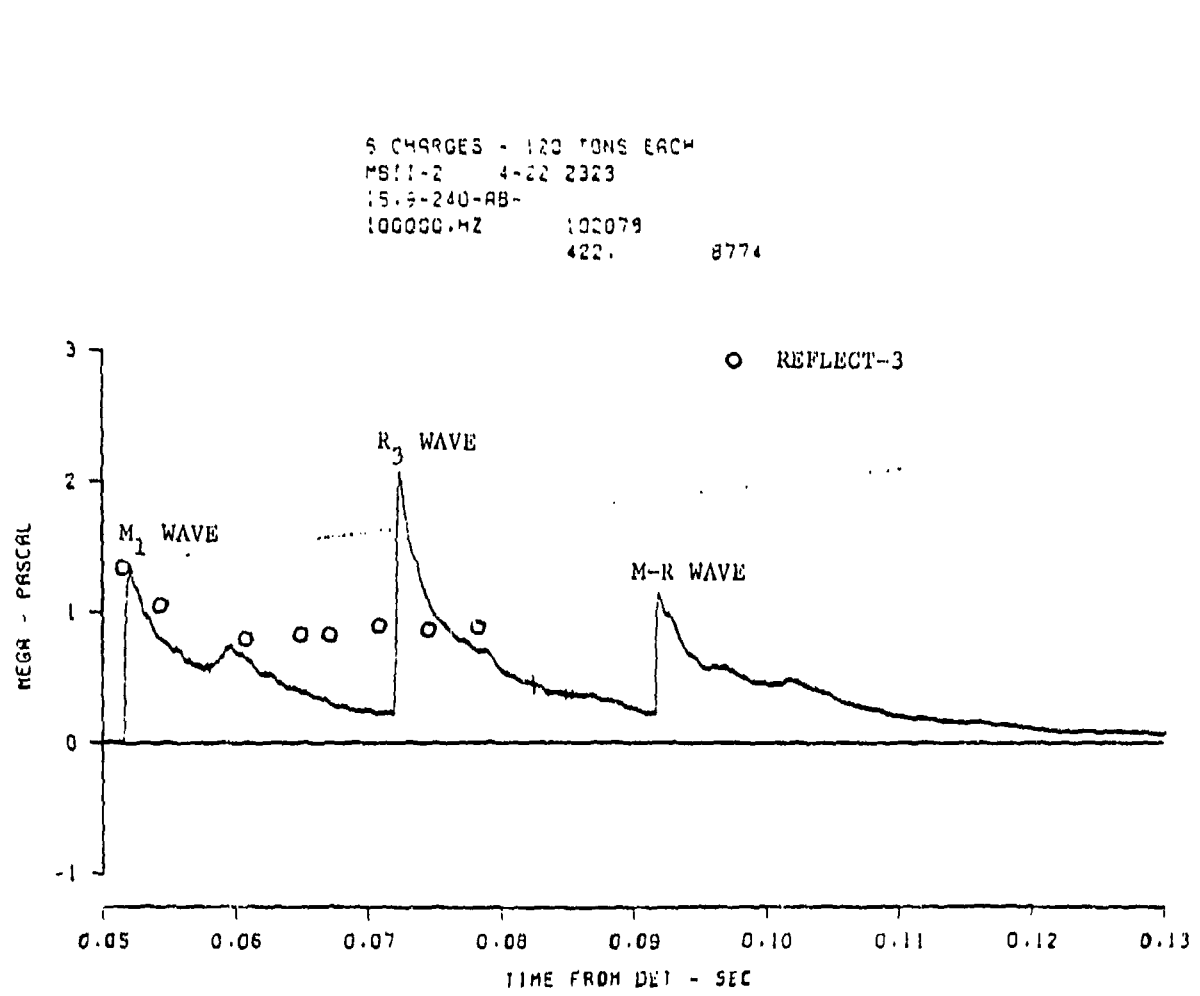

d. 52 feet from array center.

Figure 7. (Continued)

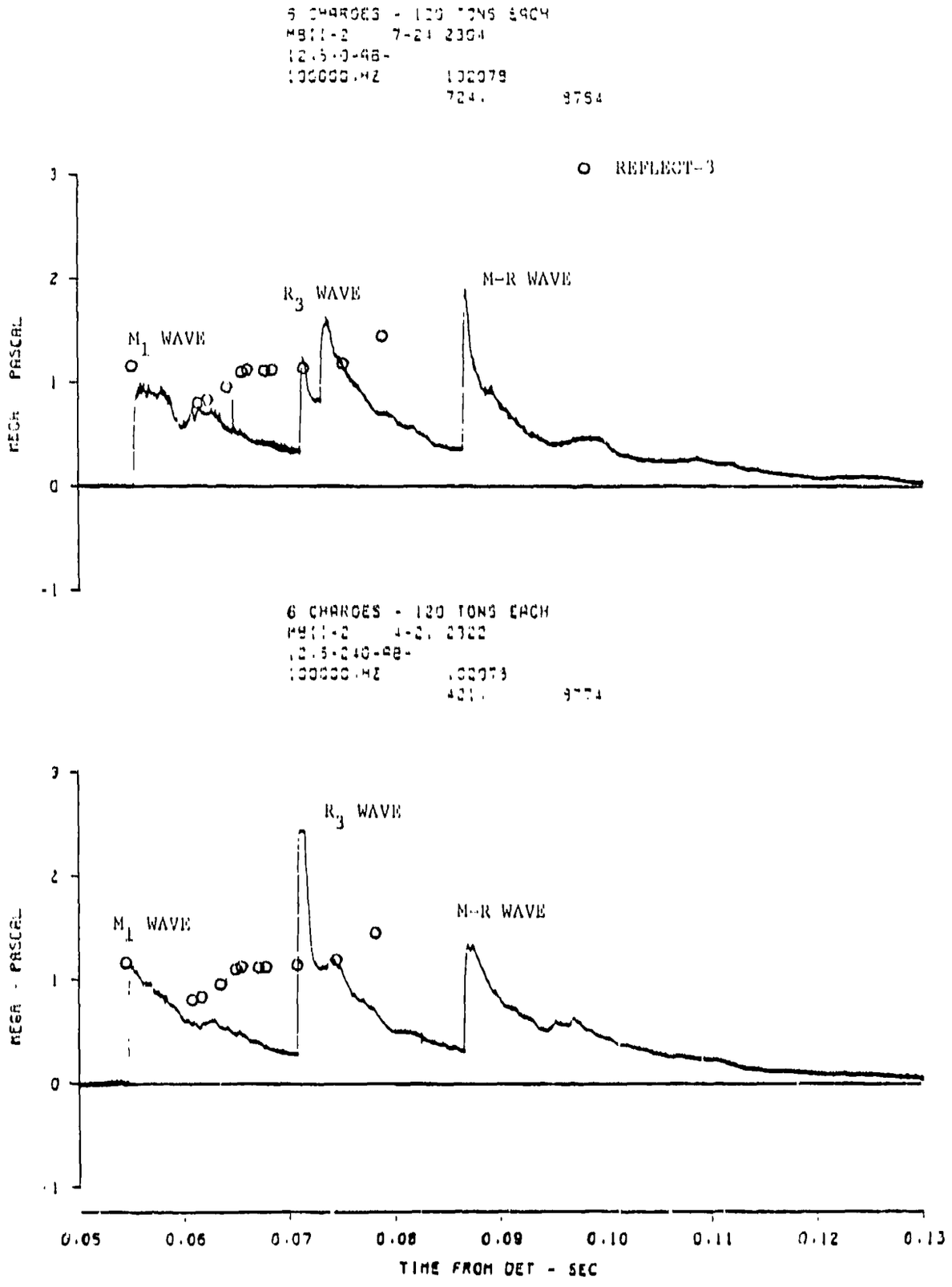

e. 41 feet from array center.

Figure 7. (Continued)

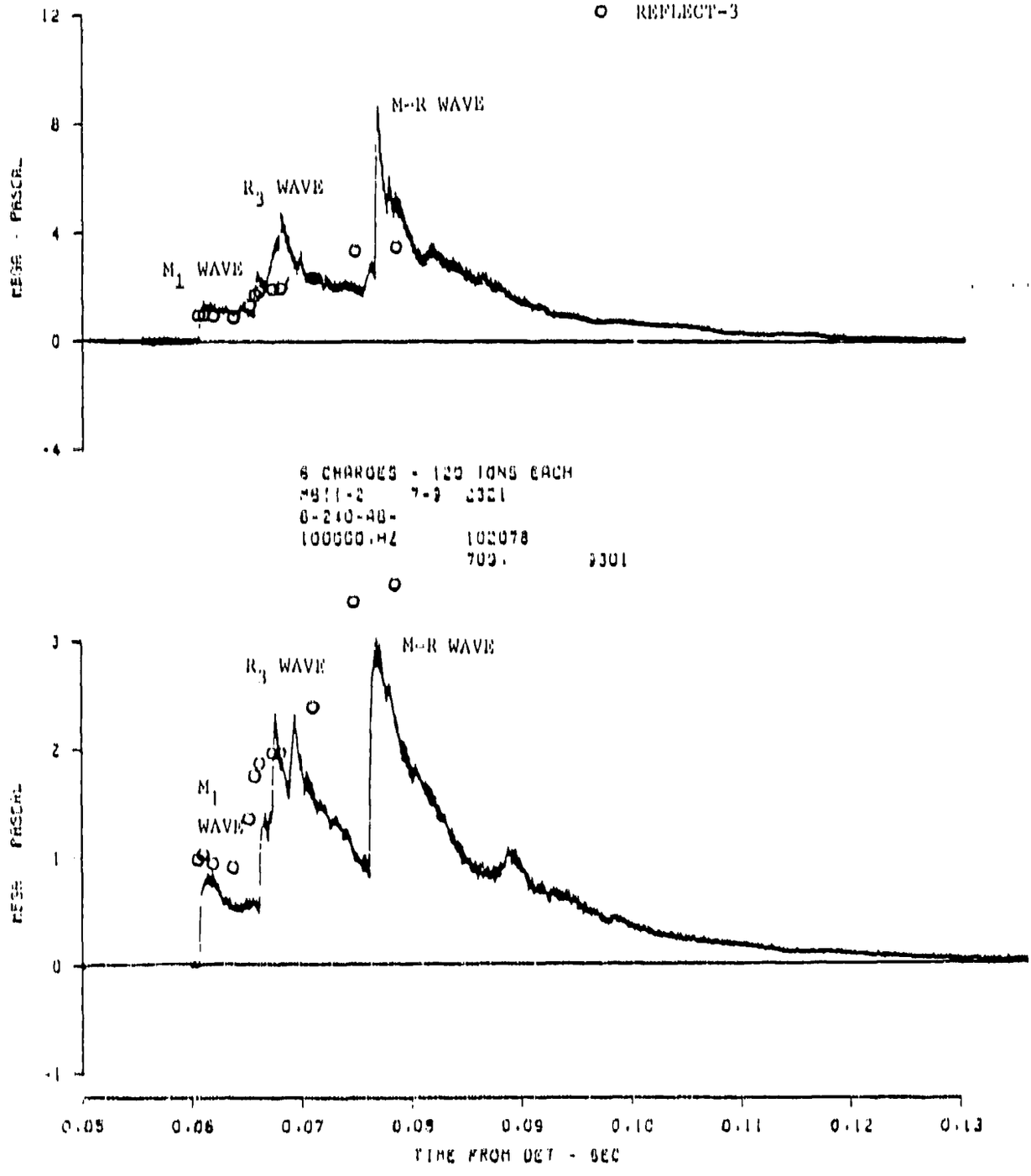

f. 20 feet from array center.

Figure 7. (Continued)

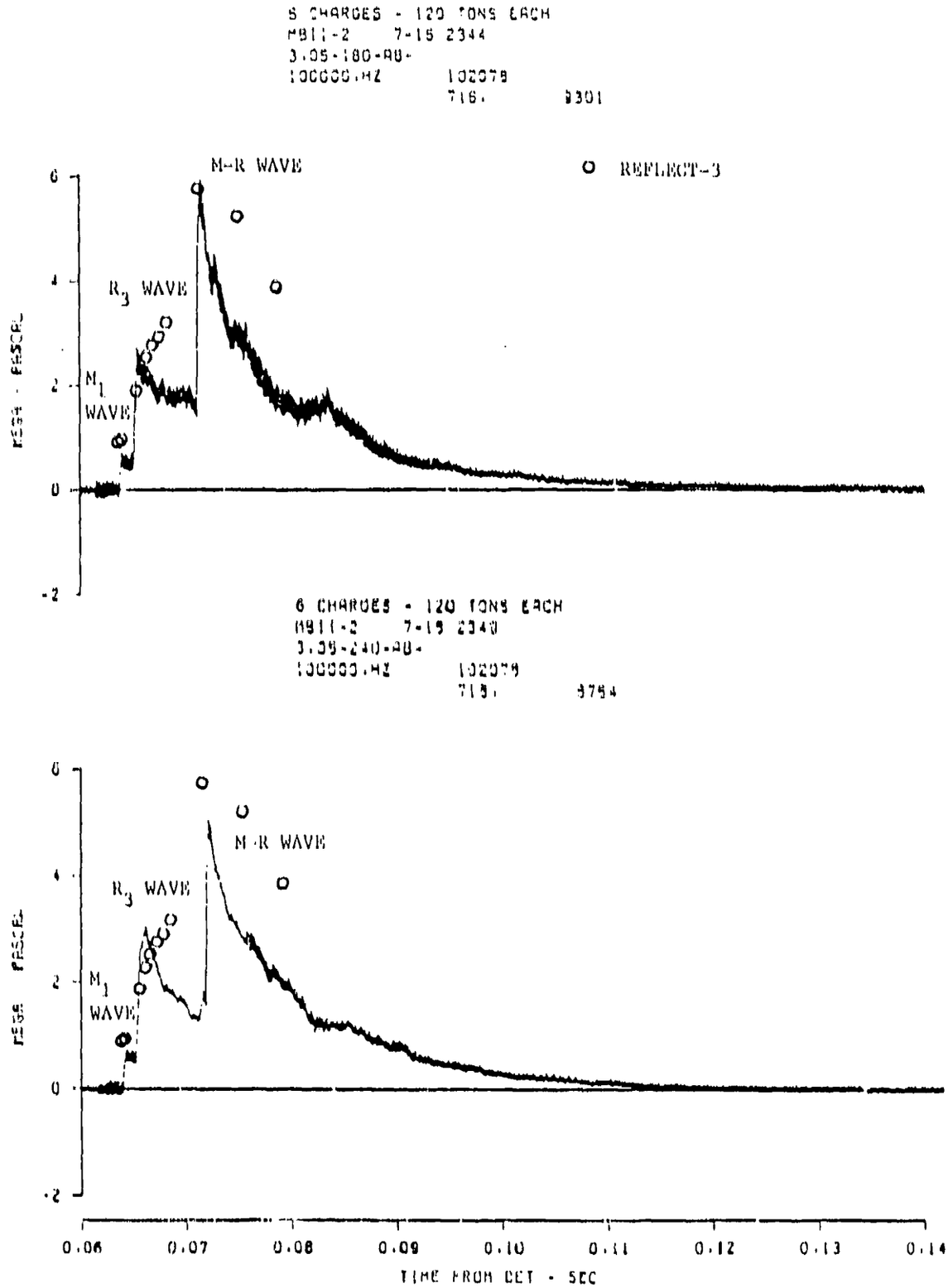

g. 10 feet from array center.

Figure 7. (Continued)

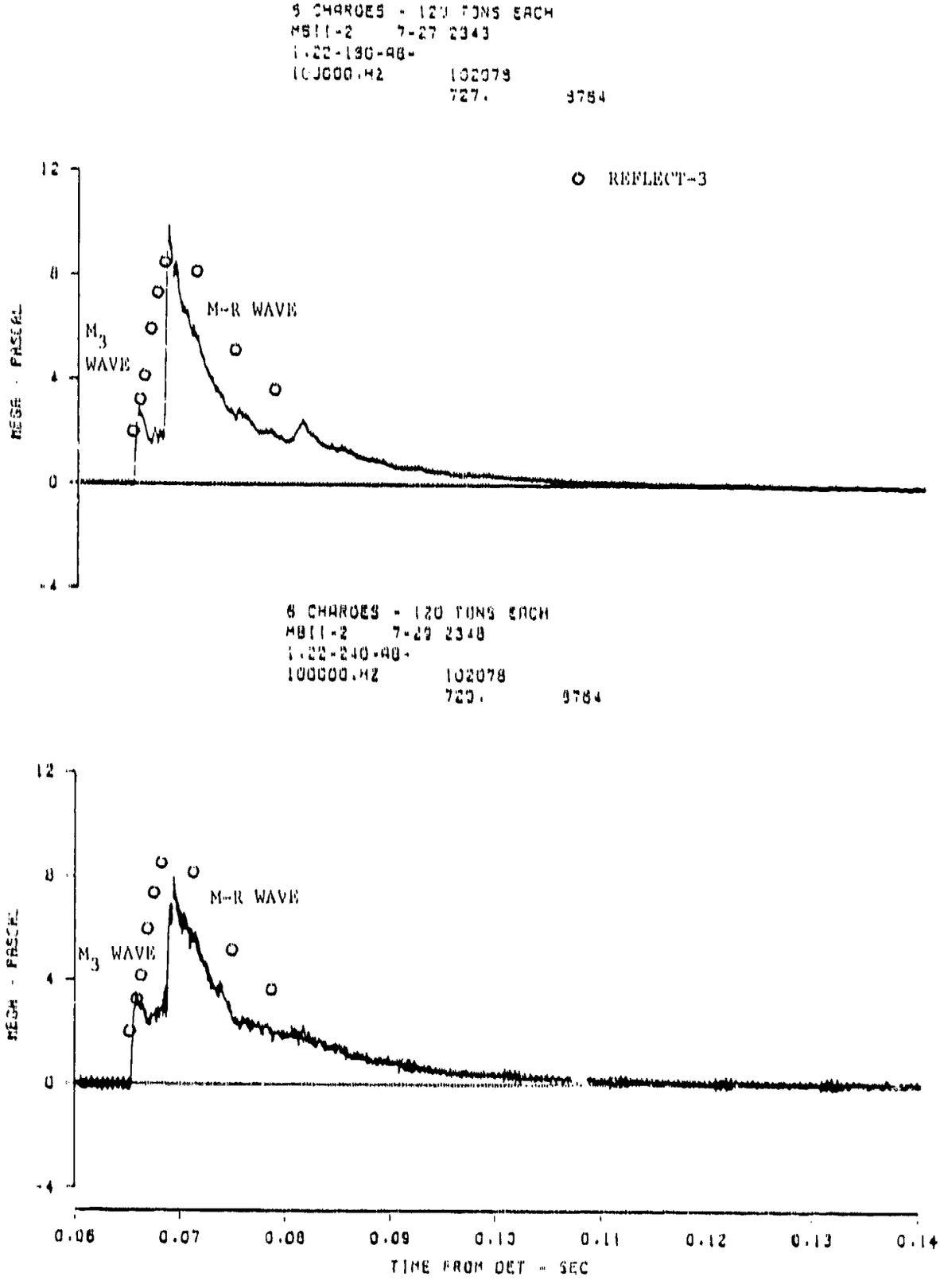

h. 4 feet from array center.

Figure 7. (Continued)

9 CHARGES - 120 TONS EACH
MBII-2 7-23 2303
0-0-AB-
100000.HZ 102078
723. 9754

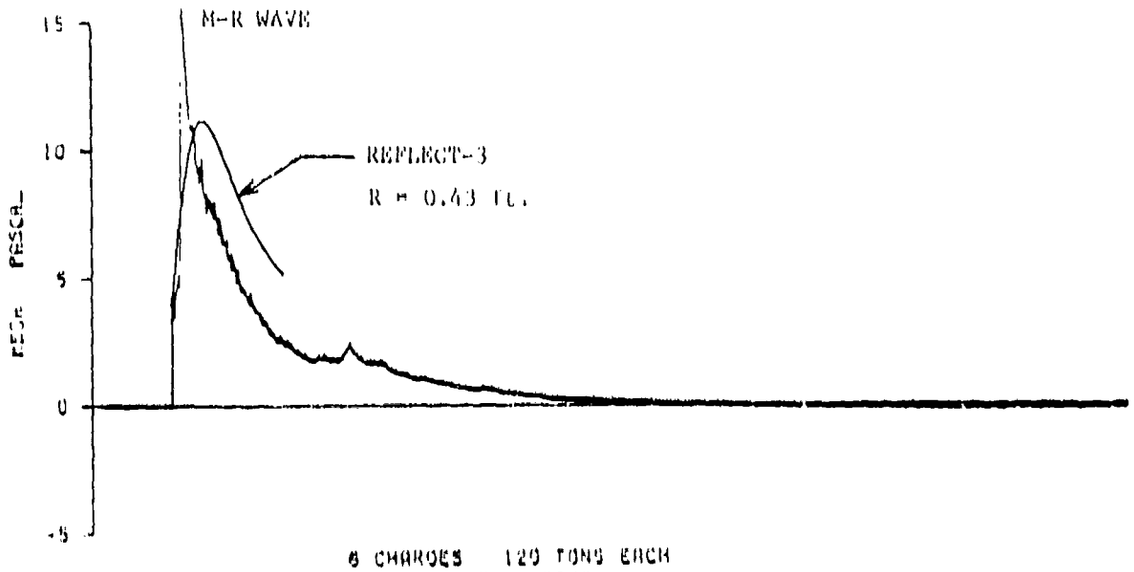

8 CHARGES 120 TONS EACH
MBII-2 7-23 2302
0-0-AB-
100000.HZ 102078
722. 9754

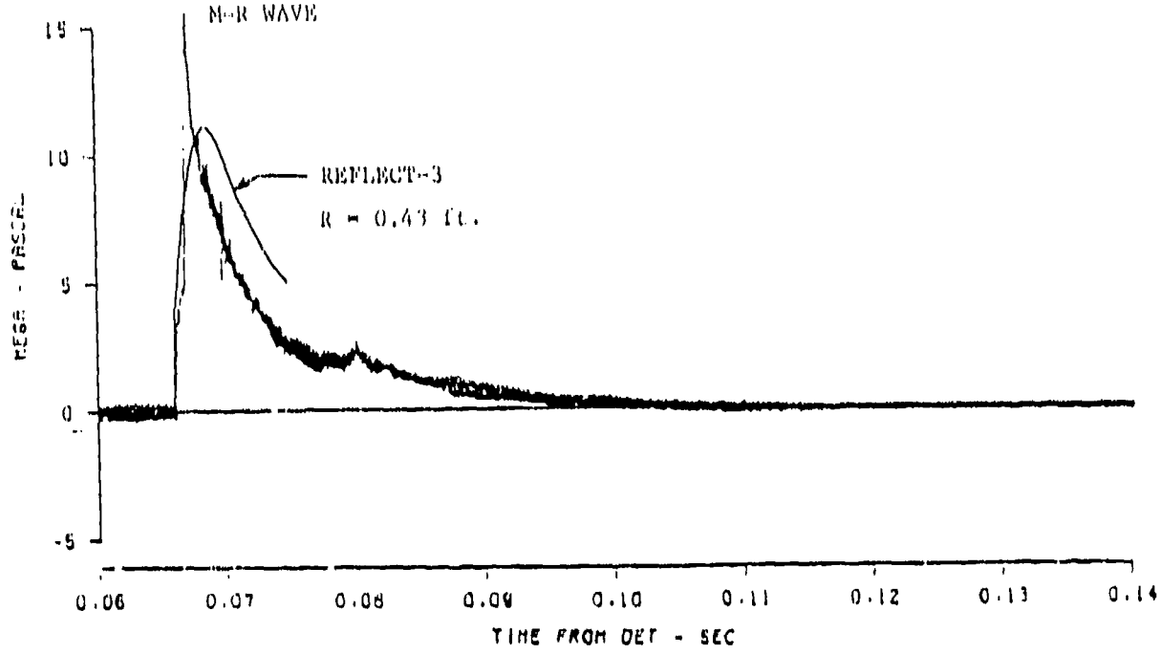

1. At array center.

Figure 7. (Concluded)

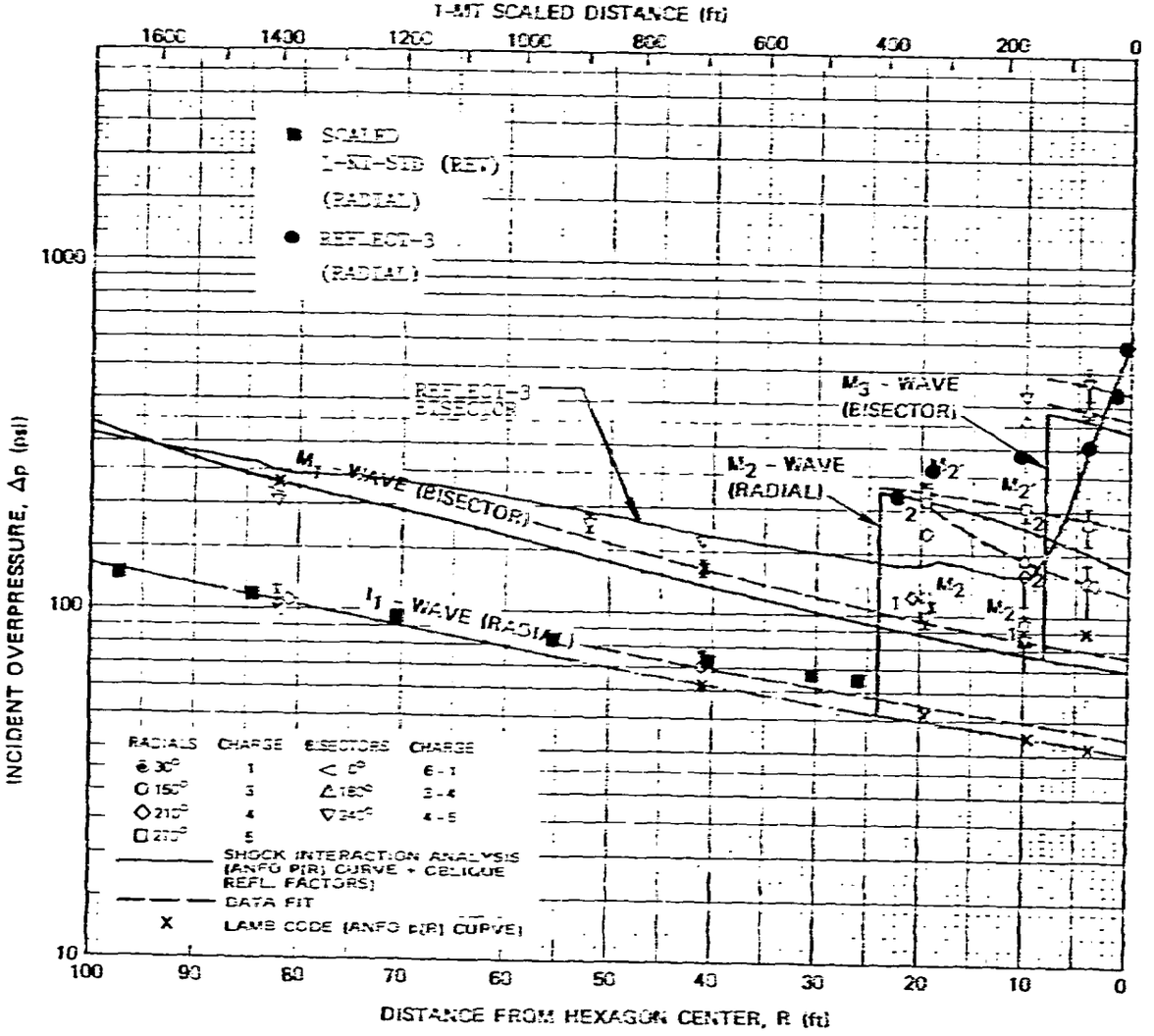

Figure 8. Comparison of incident shock overpressure predictions with MISER BLUFF II-2 test data near the array center along charge radials and bisectors.

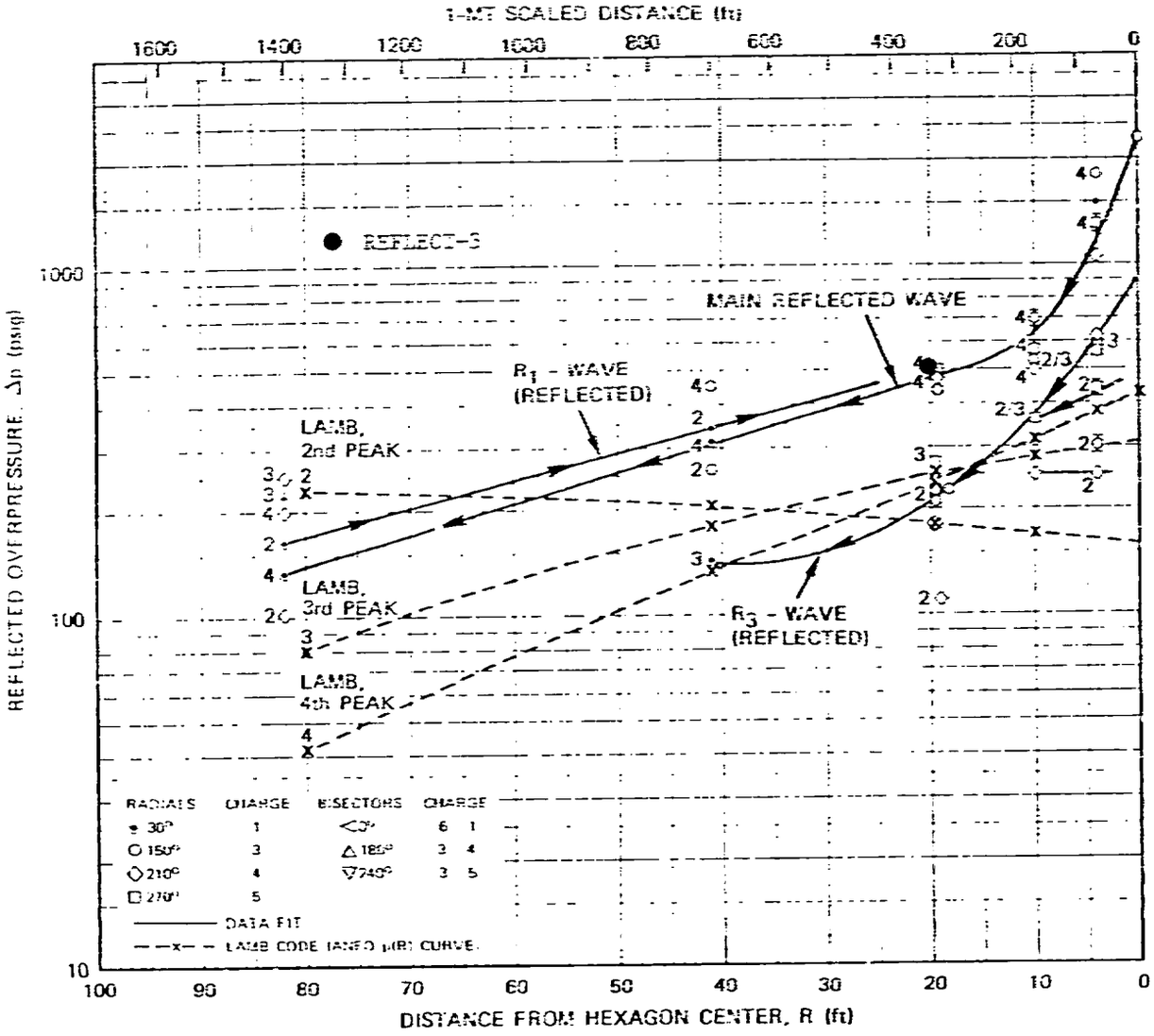

Figure 9. Comparison of peak overpressure predictions for the main reflected wave with MISERS BLUE II-2 test data near the array center along charge radials. (Arrows indicate shock wave direction; numbers indicate second, third or fourth peak.)

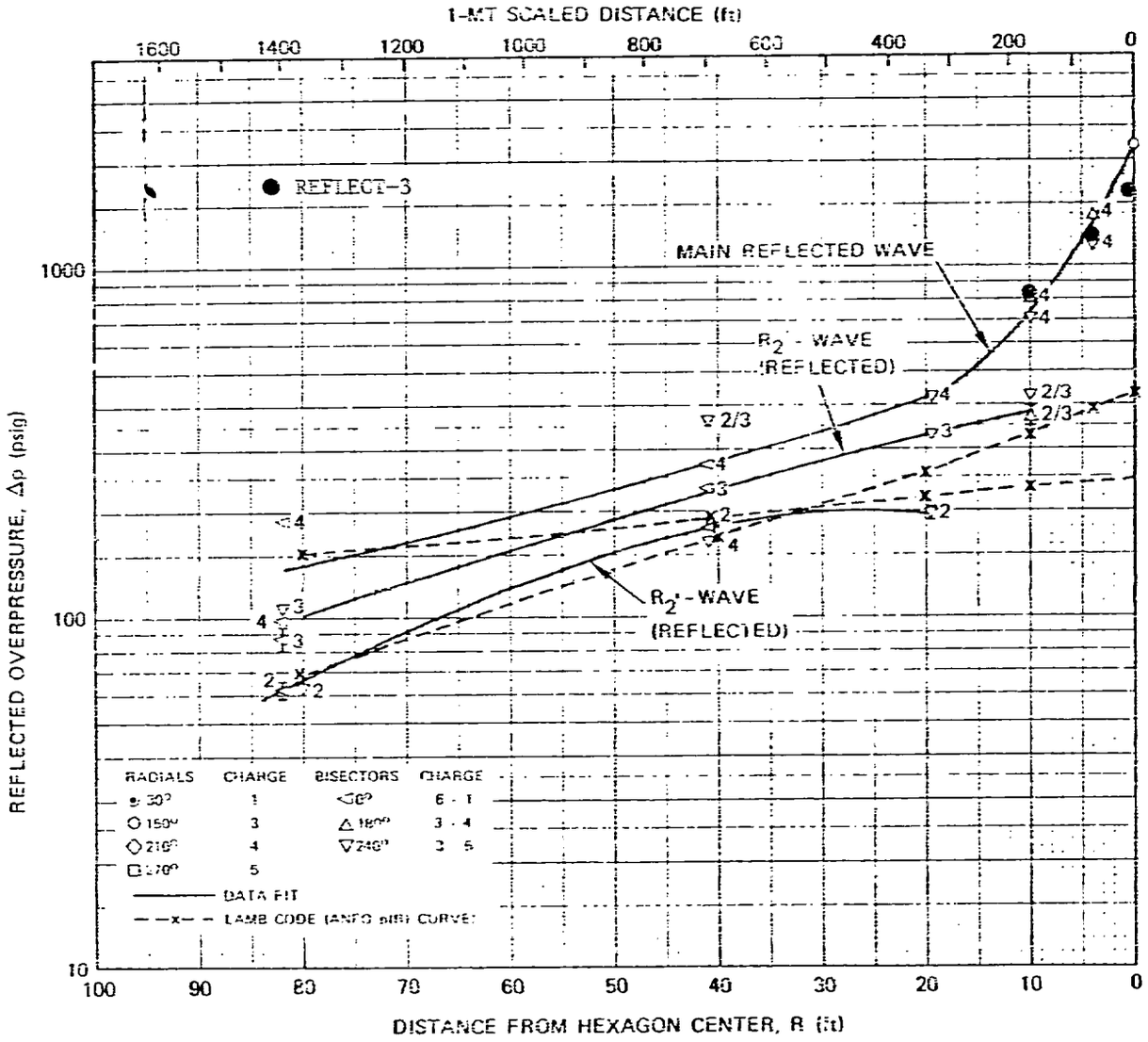

Figure 10. Comparison of peak overpressure predictions for the main reflected wave with MISERS BLUFF II-2 test data near the array center along charge bisectors. (Numbers indicate second, third or fourth peak.)

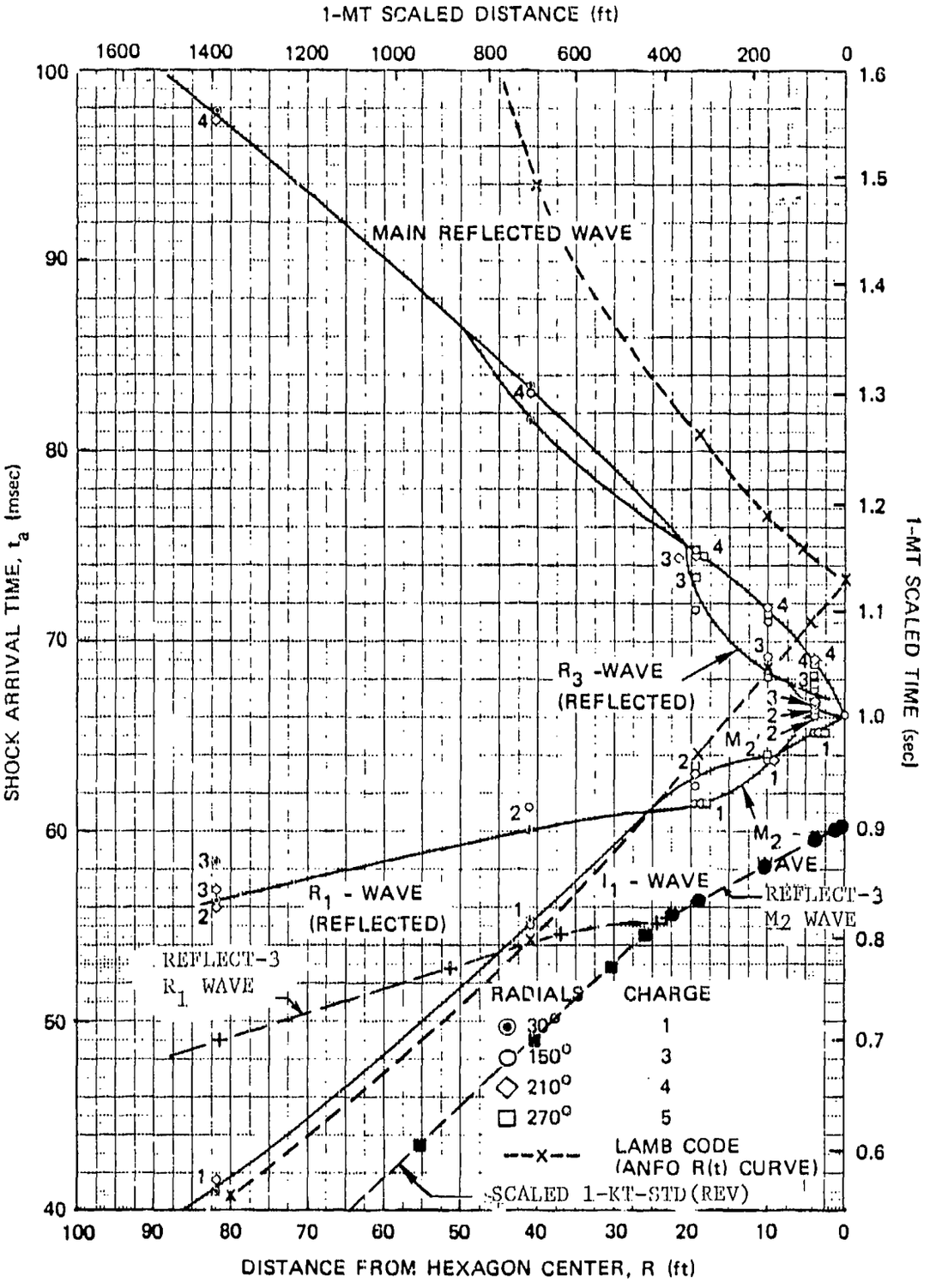

Figure 11. Comparison of shock trajectory predictions with MISERS BLUFF II-2 test data near the array center along charge radials. (Number indicates first, second, third or fourth peak. REFLECT-3 symbols ■ + ●)

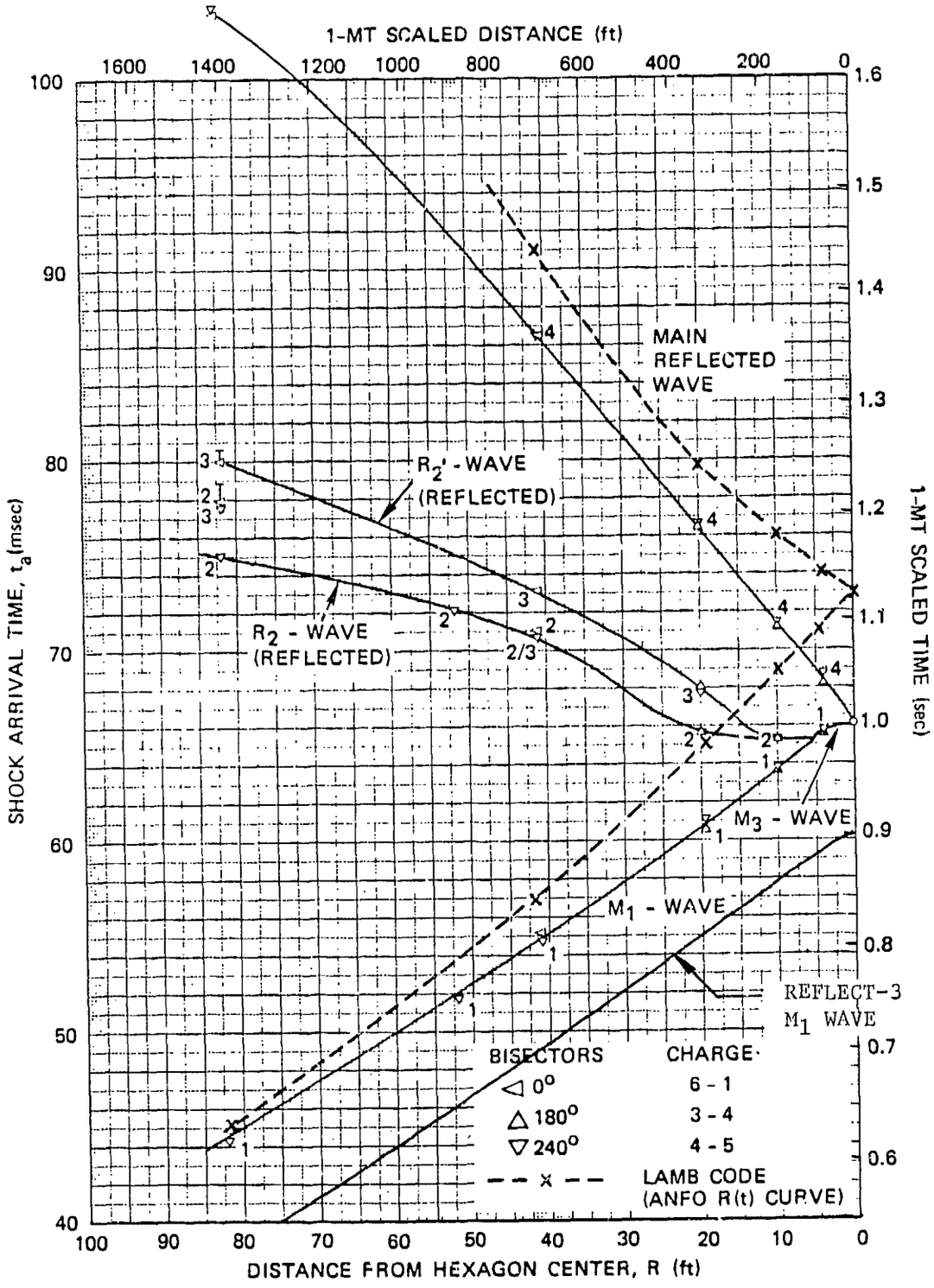

Figure 12. Comparison of shock trajectory predictions with MISERS BLUFF II-2 test data near the array center along charge bisectors. (Numbers indicate first, second, third or fourth peak.)

The second blast model was obtained from scaling the AFWL 1-KT-STD(REV) of Reference 8 for a free-air yield of 0.67 KT for the ambient conditions of the MB II-2 test. The shock overpressure for this model is also compared in Figure 5 with the MB II-2 test results. The agreement with the test data is very good at both the 82 and 41-ft stations.

3-1.2 Overpressure Wave Form.

At test stations on the radials at a distance of 82 feet from the array center, Figure 6a, the overpressure during approximately the first 0.025 seconds following the arrival of the I_1 shock is produced by the blast wave from the charge located on the radial. For this period the overpressure wave forms for the ANFO calculations and the scaled 1-KT-STD(REV) models can be compared against the test data. Two records have been used in the comparison: from Stations 25-30 (30° radial) and 25-210 (210° radial). For Station 25-30 the ANFO computed values, using at the shock the 4-point extrapolation, are about 10 percent higher (as a fraction of the shock overpressure) than the test data during about the first 10 milliseconds, they essentially agree with the test data during the middle of the period and fall about 5 percent below toward the end. The scaled 1-KT-STD(REV) values are in good agreement for the whole period.

For Station 25-210 the ANFO calculations agree fairly well with the test data. The scaled 1-KT-STD(REV) values are about 10 percent lower than the test data at early times and about 10 percent higher when the period ends (with the arrival of the R_1 wave). It is concluded from these comparisons that the waveform measurements at 82 feet from the array center support the ANFO and 1-KT-STD(REV) blast models about equally well.

Two stations were located on charge radials at 41 feet from the array center: Stations 12.5-30 and 12.5-150. The records are shown in Figure 6b. The I_1 waveform lasts only about 0.005 and 0.003 seconds, respectively, at the two stations. The record for Station 12.5-150 indicates the I_1 waveform is terminated by a double peak. Except for that the scaled 1-KT-STD(REV) values agree well with these waveform data to within the resolution of the graphs (about 0.2 to 0.4-in. amplitudes).

These comparisons on the radials provide an evaluation of the modelling of single ANFO blast waves at the ground level. From these comparisons it is concluded that the scaled 1-KT-STD(REV) blast model agrees with the test data within the data scatter at 82 and 41 feet of the array center until 0.06 seconds. There are no single-burst blast data nearer to the array center than the 41-ft station or later than about 0.06 seconds, because of the blast interactions from the other charges.

3-1.3 Selection of Scaled AFWL 1-KT-STD(REV) Blast Model.

Because of the differences in shock overpressure at the 82-ft station, it is concluded that the scaled AFWL 1-KT-STD(REV) blast model is in some what better agreement with the test data than is the ANFO calculational results. As far as the overpressure wave form comparisons, however, the two models agree about equally well with the test results.

There is another problem with using the ANFO calculational results. The properties in the region of the smeared shock must be defined and that would require some exploratory work.

Therefore the decision was made to use the scaled AFWL 1-KT-STD(REV) blast model with a free-air yield of 0.67 KT as the input to the REFLECT-3 calculations to represent the 120-ton ANFO charges used in the MB II-2 test. It is concluded that the ANFO calculational results support this blast model for use in this inner 100-ft region of the blast array within about 10 percent in shock overpressure.

3-2 R_1-M_1 WAVES.

The initial interaction of the blast waves occurs along the bisectors. The R_1 waves are produced by this interaction. A record for this interaction is shown in Figure 7a for Stations 86.6-60 and 86.6-240.

The initial shock overpressure for an 86.6-m bisector station can be calculated directly from the properties of the incident shocks by using the R-H equations. This is essentially an exact calculation, dependent upon the strength of the incident shocks. Because the two blast models (ANFO computed and scaled 1-KT-STD(REV)) were shown to agree within about 10 percent with the measurements of the I_1 shock overpressure and overpressure waveform, this calculation might be considered for use as an evaluation of the test simulation. The ANFO calculated blast wave gives an initial shock overpressure that is 7 percent higher than the scaled 1-KT-STD(REV) value at the 86.6-m station.

The test data from Station 86.6-60 has a shock overpressure that is 25 percent below the scaled 1-KT-STD(REV) value and the test data of Station 86.6-240-AB has a shock overpressure that is 36 percent below that value. Therefore it is concluded that the shock overpressures measured at initial blast intercept appear to be low by about 25 percent or more.

These differences cannot be used as a definite evaluation of the experiment because of questions regarding use of the blast models at the 164-ft (50-m) blast range. The comparisons made in Figure 5 are

for 246-ft and 287-ft blast ranges, respectively, for the 82-ft and 41-ft stations. The ANFO calculation showed a shock overpressure that tends to be high at the lower blast radius (82-ft station). The scaled AFWL 1-KT-STD(REV) shock overpressures, although they agreed at the 246 and 287-ft blast ranges, are much larger in the proximity of the burst center than for a high explosive. Therefore a definite conclusion cannot be reached at this point on the test accuracy. But the comparison does point up the possibility that the test overpressure might be low by as much as 25 percent or more compared with an ideal test.

The predicted overpressure waveform for Station 86.6-60 from the REFLECT-3 calculation are shown in Figure 7a to be within 10 percent of the test data by one millisecond after shock arrival. The differences with the test data for the 86.6-240 Station are much greater until about five milliseconds after the intercept.

The record for the 164-ft station on the charge bisector, Figure 7b, appears to indicate that one blast shock arrives about 1 1/2 milliseconds ahead of the other, tending to reduce the peak pressure. The REFLECT-3 shock value is 29 percent higher than the measured peak.

At the 82-ft stations on the charge bisector, Figure 7c, Station 25-0 has a large shock jump at 0.0448 seconds followed by a second jump about 0.003 seconds later. Station 25-240 shows a similar sequence, although the overpressure in the later case falls off about 15 percent before the second jump. The REFLECT-3 prediction essentially fairs through the test data of Station 25-0 for about 0.013 seconds after the arrival of the M_1 wave. The second jump in the overpressure may be due to an irregular type of Mach reflection. Irregular Mach reflection results in a compressive peak following the Mach shock due to the interaction of a slipline with the (virtual) reflecting surface.

At about 0.058 seconds the REFLECT-3 overpressures in Figure 7c begin to climb above the test values. This departure is attributed to the early arrival of the leading edge of the smeared R_2 shock. The R_3 wave arrives early as a result. It is expected that this effect could be eliminated by making the R_2 shock a sharp R-H shock in the REFLECT-3 code, as are the R_1 and M_1 shocks. In general, however, the predictions shown in Figure 7c are in fair agreement with the test record.

For the 52-ft station on the charge bisector, Figure 7d, the REFLECT-3 prediction agrees well with the first peak of the trace. The measured pressure trace has a slight dip until about 0.06 seconds, but the agreement with the REFLECT-3 prediction otherwise is good. Beginning at 0.06 seconds the predictions again show the effect of the early arrival of the smeared R_2 shock followed immediately by the R_3 wave.

At 41 feet on the charge bisector, Figure 7e, the REFLECT-3 prediction agrees well with the first peak measured value for the M_1 wave for Station 12.5-240 shown in the lower trace. However, the measured peak for Station 12.5-0 is about 20 percent lower and has a flat waveform for about 3 milliseconds, followed by a sudden dip, instead of the more

classical wave form of Station 12.5-240. At about 0.060 seconds the overpressure predicted by the REFLECT-3 code rises above the measured values for both the 0-deg and 240-deg stations due to the smeared R_2-R_3 wave.

The comparison for the 20-ft stations on the 240-deg bisector is shown in Figure 7f. The REFLECT-3 predictions for the M_1 wave are 25 to 50 percent higher than the measured values for Station 6-240. However the predicted values fall below the measurements of Station 6-180 by up to 25 percent. So the REFLECT-3 prediction falls between the measurements. Several factors make it appear that the calibration of the record for Station 6-180 may be in error; this will be discussed in Section 3-5. The predicted overpressures begin to rise at about 0.065 seconds due to the early arrival of the smeared R_2-R_3 wave.

3-3 R_1-R_2 WAVES.

The R_1 wave in the REFLECT-3 code reaches the radial as a sharp shock as shown in Figure 4c. It refracts across the radial as the smeared R_2 wave in the present form of the code. The R_1 shock appears to refract at the radial as a regular shock reflection. The R_2 wave following the intercept of the R_1 shock is indicated on the traces in Figure 6.

In Figure 6a the R_2 wave comparisons are shown for 82 feet from the array center. The arrival time of the R_1-R_2 wave for the REFLECT-3 prediction is within 0.0008 seconds of the measured arrival time for Station 25-30 (note: the measured variation in arrival time between the 30 and 210-deg test stations is 0.0004 seconds). This is good agreement. A second shock arrives 0.00085 and 0.0021 seconds after the first R_1 shock at the two 82-ft radial stations. The REFLECT-3 results also show a rise following the shock arrival to a second peak about 0.004 seconds later. In fact both of the test traces show a third peak a few milliseconds behind the second. The second peak may indicate a delayed arrival of one of the R_1 waves at each of the stations, and the third peak may indicate an irregular type of interaction of the shocks.

The REFLECT-3 results in Figure 6a again fair through the test data for the R_2 wave fairly well up to about 0.056 seconds. At that point the REFLECT-3 values become higher, which is attributed again to early arrival of later waves due to shock smearing. Resolution of the sharply peaked R_2 shock wave shown in Figure 6a would also require reduction in the size of the cells for the REFLECT-3 code.

Figure 6b shows the comparison at the 41-ft distance. For Station 12.5-30 the predicted arrival of the R_2-R_1 wave is 0.0010 seconds after the measured arrival, which is within the 0.00125-s difference measured between the arrivals for the two stations. Again the REFLECT-3 results fair through the test results until 0.067 seconds. The predictions then rise, which is again attributed to the wave smearing by the code, in this case by the smeared main reflected (M-R) wave.

The predictions again do not show the sharp peak of the test data, but that would require the smaller cells. The predictions do not agree quite as well with the test data for Station 12.5-150 but that station has an anomalous waveform with the two smaller waves preceding the apparent R_1-R_2 wave giving a significantly different overall waveform than for Station 12.5-30.

At the 20-ft stations on the charge radials, Figure 6c, the REFLECT-3 overpressure predictions have a waveform somewhat similar to that of Station 6-210 for about 0.004 seconds after arrival of the shock M_2. At Station 6-270 the M_2 shock is preceded by a weaker shock, whereas at the 150 (not shown) and 210-deg radials the M_2 shock arrives first. The level of the predictions is about 25 to 50 percent higher than the measured values, but there are differences of ±20 percent between the measured R_2 overpressure wave forms for the three stations at this range, so it is not clear that the measured interactions at this distance from the array center are accurate enough for much better resolution. But it does appear that the trend of the predicted values is higher than for the test data at this range.

At about 0.066 seconds the REFLECT-3 predictions in Figure 6c begin to rise significantly above the test values. This follows the trend at the more outward stations attributed to the effects of shock smearing and cell size.

3-4 R_2-R_3 WAVE.

The R_2 wave intercepts the charge bisector and reflects (regular) as an R_3 shock, as shown in Figure 4c. Both shocks are smeared in the REFLECT-3 code. The R_3 wave appears at the 82-ft stations shown in Figure 7c, but it occurs too late for complete comparison with the test data. Comparison of the REFLECT-3 results with the R_3 wave form in Figures 7d to g show that the REFLECT-3 wave is smeared and would need a sharp R_2 shock and smaller cells to reproduce the relatively sharp peak of the R_3 wave.

Figure 4c shows that stations on charge bisectors within 9 feet of the array center would be expected to have the Mach shock M_3 arrive first. Careful inspection of the trace for Station 1.22-180 shows a steep initial shock jump very nearly equal to the REFLECT-3 shock jump indicated by the first point. The REFLECT-3 values continue to climb as do the test data, but the REFLECT-3 values continue to climb due to the early arrival of the smeared M-R wave. The initial shock jump is not quite as distinct for the trace of Station 1.22-240, but the REFLECT-3 results compare similarly.

3-5 M-R WAVE.

The blast waves from charges that are located more than 90 degrees away around the hexagon produce the wave identified here as the M-R wave, taken again from the terminology in Reference 1 where it is called the main reflected wave. For points on the radials, as shown in Figure 6, the M-R wave is produced by three charges. For points on the bisectors, as shown in Figure 7, it is produced by two charges.

At the stations within 20 feet of the array center the M-R wave arrives early enough to allow comparisons of the REFLECT-3 results. These comparisons are shown in Figures 6c and 7f to i.

The M-R wave predicted by the REFLECT-3 code is of course smeared, but, with one exception, the magnitude of the peak overpressures generally agrees fairly well with the test results. The exception is for Station 6-180 which is believed to have an erroneous calibration, which is supported by several other features (the rapid decrease in the overpressure of the M_1 shock along the 240-deg charge bisector that would result between 20 and 10 feet of the array center and by comparison of results with those for Station 6-240).

3-6 ARRAY CENTER.

The comparison for near the center of the array is shown in Figure 7i. The REFLECT-3 results are for a point on the bisector 0.43 from the array center. The M_3 shock jump predicted by the REFLECT-3 code is 570 psi (3.93 megapascals). It compares well with the shock jump measured at the two stations, as indicated by the first sharp rise.

The peak overpressure predicted by the REFLECT-3 code at 0.43 feet is 1615 psi (11.1 megapascals), which is 71 percent of the peaks of about 2260 psi (15.6 megapascals) measured from the records of the two stations in Figure 7i at the array center. This is very good agreement in view of the relatively large size of the cells employed in the REFLECT-code and the smearing of the R_2 and R_3 shock waves. The wave form of the REFLECT-3 overpressure is relatively similar to the measured wave form of the M-R wave except for the greater width and reduced peak. The comparison is very encouraging for the potential of the code.

3-7 INCIDENT SHOCK OVERPRESSURES.

The shock overpressures for the incident shock at points on radials and bisectors within 100 feet of the array center are plotted in Figure 8 reproduced from Reference 1. The REFLECT-3 values are plotted for comparison.

The REFLECT-3 radial values from 100 feet inward to 26 feet are the scaled 1-KT-STD(REV) input values to the code, so they do not provide a comparison for code evaluation. On the bisector at 82 feet the REFLECT-3 values are about 10 to 25 percent higher than given for the test data. However the test data, Figure 7e, have a second peak occurring only about 0.003 seconds after the incident shock, and the REFLECT-3 value is only 7 percent higher than the second-peak value for Station 25-0-AB.

At 52 feet on the bisector the REFLECT-3 values agree with the test peak value. At 41 feet on the bisector the REFLECT-3 shock overpressure agrees with the test value for the 240-deg station. The shock value for the 0-deg station is lower by 16 percent, but this record, Figure 7e, has a peculiar waveform, so the value is questioned.

At 20 feet on the bisector the predicted value of 140 psi falls between the measured values of 93-107 psi and 188-210 psi for the 240 and 180-deg bisectors, respectively. However, the calibration of the latter record appears questionable, as discussed in Section 3-5, so the prediction may be slightly high. The REFLECT-3 curve for the bisector in Figure 8 had a small rise between the 22 and 18-ft stations. This rise is attributed to the advance arrival of the smeared M_1-R_2-M_2 triple point. At 10 feet on the bisector the predicted values are shown in Figure 6 to be about 30 percent higher than the measured peak values from the 180 and 240-deg bisectors.

At a distance of about 9 feet from the array center the REFLECT-3 incident shock overpressure on the bisector begins to climb. This corresponds with the presence of the M_3 wave shown in Figure 4c. Because the R_2 and R_3 waves are not modelled in REFLECT-3 at this time as R-H shocks, the predicted incident shock overpressure increases smoothly instead of with the shock jump that would be expected in the actual case. At 4 feet from the array center the predicted incident shock overpressure is about two-thirds of the values reported in Reference 1. However, the record for Station 1.22-190 has a steep initial rise that corresponds well with the REFLECT-3 value, and this rise may be the actual M_3 shock, and the value reported in Reference 1 may be that of a peak after the M_3 shock arrival.

The REFLECT-3 shock overpressure on the radial for the incident shock reaches 593 psi when the shock is 0.49 feet from the array center. At that point the cell system was frozen. On the bisector the incident shock was within 0.43 feet of the array center with an overpressure given by the REFLECT-3 code of 570 psi.

It is concluded that the incident shock strengths on the bisectors are predicted well into 41 feet. From 20 to 10 feet the predictions appear to run somewhat high by as much as about 30 percent, which may be due to early arrival of the R_2 wave due to smearing. At 4 feet the REFLECT-3 results appears to agree well with the data. The same agreement also exists near the array center. So, the REFLECT-3 results for the incident shock overpressure on the radial appears to agree well with what are believed to be the best data, except where smearing of the R_2 wave appears to produce higher predicted overpressures.

Along the radial the REFLECT-3 incident shock overpressure is seen in Figure 8 to increase at about the 24-ft station where the M_2 wave shown indicates a jump. Again, the incident shock in the REFLECT-3 model is a R-H shock but the reflected R_2 wave is diffuse, so the rise would be expected to be not as sudden as in the test. At 22 1/2 feet the REFLECT-3 value agrees with the shock interaction analysis prediction of Reference 1. At the 20-ft station the REFLECT-3 incident shock overpressure is about 25 to 50 percent higher than the measured peak values. However, as mentioned in Section 3-3 there are significant

differences in the waveforms measured on the three radials (150, 210 and 270 degrees, Figure 6e). In fact, the waveform for the 210-deg radial continues to climb after shock arrival reaching a peak only 0.0018 seconds after shock arrival that agrees well with the predicted shock overpressure. On the 270-deg radial it appears the M_2 wave has not overtaken the incident shock at the 20-ft station.

The REFLECT-3 predicted incident shock overpressure on the radial, Figure 8, continues to increase gradually to about the 3-ft station. At the 10-ft and 4-ft stations it is about 50 to 115 percent higher than the measured peak values, but comparisons with the test wave forms have not been made. At 4 feet the measured shock overpressures range from 102 to 522 psi (Reference 1) and the REFLECT-3 value is 305 psi. At the 3-ft station the REFLECT-3 value reaches essentially the same value as on the bisector and remains nearly the same inward to 0.49 feet from the array center where the mesh was stopped.

It is concluded that the incident shock strength is predicted well where the M_2 shock first forms at about the 24-ft station. The REFLECT-3 value continues to climb whereas the test values decrease inward to the 10-ft station, but the differences are unresolved. From 4 feet inward the predictions are supported by none of the test results, but the test results differ significantly.

3-8 MAIN REFLECTED SHOCK OVERPRESSURES.

Shock overpressures predicted for the main reflected wave by the REFLECT-3 code are compared with the MB II-2 data in Figures 9 and 10. For the charge radial there is one point for comparison which is at 20 feet. The agreement with the test results is excellent.

For the charge bisector, Figure 10, there are predictions for three locations to 10 feet. The agreement at 10 and 4 feet is excellent. At 0.43 feet the prediction is about 23 percent low. It is believed that a smaller cell size would improve the prediction, particularly because of the steepness of the peak (Figure 71).

3-9 SHOCK FRONT TRAJECTORIES.

The predicted trajectory of the incident shock along a charge radial is compared with the test data in Figure 11. Inward to the 23-ft station the velocity is that given by the scaled 1-KT-STD(REV) model. The shock velocity agrees with the test data in this range, which serves essentially as a consistency check because the predicted overpressures were found to agree there with the test data. The shock arrival time for the scaled 1-KT-STD(REV) model is about 6.6 milliseconds less than measured, which is expected as it is a nuclear blast wave model.

Between the 24.5-ft station and the array center the predicted shock velocity along the radial increases because of the greater strength of the M_2 shock that forms at 24.5 feet. The REFLECT-3 M_2

shock is generally stronger than measured, but by the time the incident shock is near the array center the separation in arrival time between the predicted shock and the test data has decreased by about 0.6 milliseconds.

The shock front trajectories along the bisectors are compared in Figure 12. At the 82-ft station the REFLECT-3 shock arrives ahead of the test shocks by about 6.2 milliseconds. The separation decreases slightly, to about 6.0 milliseconds at about the 50-ft station, and it remains essentially constant from there on inward to the array center. It is noteworthy that the predicted speed of the incident shock increases in the final few feet from the center roughly similar to the speedup shown by the test data.

SECTION 4
DISCUSSION

The overpressure measurements from the MIGHTY MACH II-2 (MB II-2) six-burst test have been employed here as the basis for evaluation of the REFLECT-3 code results. Before reviewing the comparison, a few comments are noted regarding the use of the test results.

The detonation of six large high-explosive charges to produce blast waves sufficiently identical in space and time to converge at the array center with the accuracy that might occur for nuclear explosions is a difficult technical task. Evidence of the problem can be seen in the differences obtained in the overpressure histories measured on different bisectors for the interaction of simply two blast waves, Figure 7a. The shock overpressure for the pair intercepting on the 240-deg bisector is 36 percent lower than for the pair intercepting on the 60-deg bisector, and the latter is 25 and 30 percent below the two values computed from the blast models (Section 3-2).

The overpressure test records are presented in Figures 6 and 7 grouped in pairs by similar locations for comparison purposes. The differences between traces for any one pair is readily apparent. The differences are in arrival time, waveform and magnitude.

Many of the differences that could be expected between the blast waves themselves — such as time of arrival, sphericity, etc. would generally be expected to tend to lower the interaction overpressures. A hydrocode calculation, on the other hand, having identical blast waves and that employed accurate hydrodynamic modelling -- such as "sharp" Rankine-Hugoniot shock waves, sufficiently small cell or mesh sizes, etc. — would be expected to give overpressures that would occur under ideal burst and atmospheric conditions. A good hydrocode calculation is expected to serve in defining the upper limit of overpressures that could be expected for blast wave interactions, in particular for nuclear bursts.

The REFLECT-3 code in its present form is expected to be most accurate prior to interaction of the refracted R_1 waves at the charge radials. This period terminates with the intereception of the triple point I_1-R_1-M_1 and the charge radial, Figure 4c, which is predicted to occur on radials at 24.5 feet from the array center. During this period the shock overpressures predicted along a charge bisector for the incident shock M_1 are found to agree well with the maximum overpressures measured from 82 feet inward to 41 feet in the MB II-2 tests, Figure 8. The 24.5-ft intercept of the triple point and the charge radial is in good agreement with the 24 feet predicted by Kuhl (Reference 1) and the test results. Definite conclusions regarding the overpressure wave forms predicted for this period cannot be made because of some anomalies in the test data for points on the charge bisectors, Figures 7a-e.

However there is good agreement between the predicted wave form and one test record, for the point of first intercept at 284 feet on the 60-deg charge bisector, Figure 7a, starting at one millisecond after shock arrival, and there is supportive agreement with other records.

The REFLECT-3 prediction of the R_1-shock arrival time for points on the charge radial is in good agreement with the test results for the 82 and 41-ft stations, Figures 6a-b. The REFLECT-3 prediction has the shock jump at the beginning of the R_2 wave, because it employs the sharp R_1 shock. The test records show a very sharp pressure spike for this R_2 wave following the shock and the predicted results essentially fair through these wave forms. Resolution of the overpressure peak would require some reduction in the cell sizes used in the code.

The R_2 and R_3 shocks (Figure 4e) have not been modelled in the present form of the REFLECT-3 code as sharp Rankine-Hugoniot shocks, so these shocks become smeared over several cells in the results. This smearing causes the pressures ahead of these shocks to rise early. For example, the rise of the incident M_1 shock overpressure predicted along a charge bisector, Figure 8, commencing at the 22-ft station and amounting to about 10 percent is attributed to this R_2-shock smearing effect. The predicted incident shock overpressure is found to be higher than measured by up to 30 percent from 18 1/2 feet inward to 10 feet which is attributed in part to the smeared R_2 shock. The marked climb in the M_1 shock overpressure commencing at the 9-ft station is associated with the arrival of the bulk of the smeared R_2 shock.

The R_2 shocks intercepting at a charge bisector form the R_3 waves. The early arrival of the leading edge of the smeared R_2 waves appears to affect the predicted overpressure wave forms at stations on the bisector from 82 feet inward to 10 feet, Figure 7c-g. From 82 feet inward to 42 feet it appears to cause a pressure rise about 0.01 to 0.02 seconds early, beginning at about 0.06 seconds. At 20 and 10 feet the overpredictions beginning immediately with the arrival of the incident M_1 shock are attributed to it.

After the predicted formation of the incident M_2 shock (at 24.5 feet) on the radial and the incident M_3 shock (at 9 feet) on the bisector, the incident shock overpressure predicted by the REFLECT-3 code climbs monotonically along both the radial and the bisector inward to the array center, Figure 8. This result is in contrast to the trend given by the shock interaction analysis of Reference 1 of decreasing shock overpressures.

Relative to this question the test results show the following. The predicted incident shock overpressure at 22.5 feet on the radial agrees well with the prediction of Reference 1 and the test results at 20 feet, Figure 8. Comparisons of predicted wave forms and test records have not been made for the radial inside of 20 feet, so an evaluation cannot be given. At 10 feet on the bisector the advance arrival of the

smeared R_3 shock affects the comparison. But by 4 feet this effect would be expected to be essentially over, and at 4 feet and 0 feet the predicted incident shock overpressure agrees well with the test results, Figure 7h-i. It is concluded from this comparison that the strength of the incident shock increases after the M_2 and M_3 shocks are formed, but the conclusion is tentative, dependent upon calculations with sharp R_2 and R_3 shocks and smaller cells.

The main reflected (M-R) wave formed from the implosion of all six blast waves at the array center is of primary concern as it results in the highest overpressures observed, Figures 9 and 10. At 0.43 feet from the center the peak overpressure predicted for the M-R wave by the REFLECT-3 code is about 23 percent lower than measured, Figure 10. At 4 feet on the bisector the predicted value falls slightly below the data and at 10 and 20 feet on the bisector and radial, respectively, it lies somewhat above. There is therefore a trend for the predicted peak overpressure of the M-R wave to decrease more slowly than for the test results and to be higher at the further distances than measured in the test.

The test records indicate a rather sharp peak for the M-R wave, particularly for the array center. The predicted M-R wave forms are stretched out more in time. This stretch-out is expected to affect the peak value predicted. The stretch-out is attributed to the finite cell size, and it is expected to have a greater effect on the comparison close to the array center where the cell dimension becomes more important and the test record indicates the most rapid decay timewise.

A reduction in the cell size used in the REFLECT-3 code would tend to raise the peak pressures predicted in the M-R wave. the increase could well result in raising the peak pressures of the M-R wave at all distances from the center. In fact, the predictions might well then all fall well above the measured peak overpressures. Without further information on the characteristics of the imploding shock segments in a multiple-burst event relative to the effects of non-uniformity in blast detonations, atmospheric and terrain effects, etc., it is reasonable to speculate that perhaps higher peak overpressures might be attainable. This possibility is supported by the rapid decay indicated in the measured overpressure in Figures 9 and 10, a factor of two in a distance of only 4 to 6 feet, Figures 9 and 10, which might imply stringent time-of-arrival requirements.

In general it is concluded that the potential of the REFLECT-3 code has been well demonstrated in these comparisons with the MISERS BLUFF II-2 data. The two improvements to the code that have been indicated throughout are (1) to represent the reflected shocks R_2 and R_3 as sharp Rankine-Hugoniot shocks, as are the R_1 reflected shock and the three incident Mach shocks, M_1, M_2 and M_3, in the present REFLECT-3 code, and (2) to reduce the cell sizes for better wave form definition.

SECTION 5
CONCLUSIONS

The REFLECT-3 code has been developed by making limited modifications to the original REFLECT code (DNA Report No. 3470F). The objective has been to determine from comparisons with the test results of the MISERS BLUFF II-2 event the potential of the code, if modified, for computing the interaction of multiple nuclear blast waves from ground-level detonations. The MISERS BLUFF II-2 test consisted of the simultaneous detonation of six 120-ton ANFO charges placed in a hexagonal array with 100-ft separations. The following conclusions were reached from the comparisons.

1. Between 100 and 41 feet of the array center the predicted incident shock overpressures for the charge bisector agree well with the maximum values measured.

2. Within about 22 feet of the array center the smearing of the R_2 and R_3 refracted shocks affects the predictions of the incident shock overpressure. Overpredictions relative to the test results of up to 30 percent are observed. Within 4 feet of the array center, where the smearing effect may be less, the predictions agree well with the incident shock overpressures measured.

3. The peak overpressure predicted for the main reflected wave is 1615 psi at 0.43 feet from the array center (the closest point from the center computed), which is only about 23 percent below the test result. At 4, 10 and 20 feet from the center the agreement is very good. Based on considerations concerning the code calculations and test factors, it is possible that higher overpressures might be obtainable than measured; it is expected that they could be adequately predicted following code improvements indicated below.

4. The two improvements to the code that have been indicated throughout are (i) to represent the two reflected shocks R_2 and R_3 as sharp Rankine-Hugoniot shocks and (ii) to reduce the sizes of the cells.

REFERENCES

1. Kuhl, A.L., Airblast Cumulation near the Center of Symmetry for Six ANFO Charges, RDA Report RDA-TR-110006-003, April 1979.

2. Ruetenik, J.R., Thompson, J.H, Dalton, T.A., and Lee, W.N., REFLECT Computer Code for Ground-Reflected Blast Waves, Kaman AviDyne Report TR-96, Defense Nuclear Agency Report No. 3470F, 21 April 1975.

3. Godunov, S.K., A Difference Method for Numerical Calculation of Discontinuous Solutions of the Equations of Hydrodynamics, Mat. Sb. 47, p. 271-306, 1959.

4. Brode, H.L., Theoretical Descriptions of the Fireball, Blast and Thermal Radiation from a Nuclear Explosion at 60,000 ft., The RAND Corp., August 1965, Unpublished.

5. Air Force Weapons Laboratory MISERS BLUFF Tape No. IE2.

6. Private communication from C.E. Needham, Air Force Weapons Laboratory, to J.R. Ruetenik, 18 October 1979.

7. Private communication from C.E. Needham, Air Force Weapons Laboratory, to J.R. Ruetenik, 12 June 1979.

8. Needham, C.E., Havens, M.L., and Knauth, C.S., Nuclear Blast Standard (1 KT), Air Force Weapons Laboratory, Report AFWL-TR-73-55 (Rev). April 1975.

9. Smiley, R.F., Ruetenik, J.R., and Tomayko, M.A., FAB-2D Computations of Nuclear Free-Air Blast Waves in a Horizontally Stratified Standard Atmosphere, Kaman AviDyne Report TR-166, Prepared for the Defense Nuclear Agency.

10. Zartarian, G., and Lee, W.N., Program REFRA - Blast Routine Based on REFLECT Code, Kaman AviDyne Report TR-102, DNA Report 3596F, 2 May 1975.

APPENDIX
THE PFAB CODE

GENERAL DESCRIPTION OF CODE.

The PFAB computer code was developed as a modification of the FAB-2D code of Reference 9 for computing the main reflected wave in the six-burst problem. The method employed is to solve the planar two-dimensional transient fluid-flow problem of the reflection of an initially prescribed blast flow from the corner of a wedge-shaped boundary, as indicated in Figure 13.

The flow field outside of the computational cell system shown in Figure 13 is a prescribed time dependent flow, which is in the present application given by the REFLECT-3 code. While the REFLECT-3 code does compute this same problem as part of its late time solution, the PFAB code is more realistic in that the main reflected blast wave is represented as a sharp Rankine-Hugoniot shock front (which is smeared in the REFLECT-3 code) and the PFAB geometric cell layout is better adapted to the features of the main reflected wave.

The code computes the flow in a moving cell coordinate system similar to the one shown in Figure 13. The cell system consists of an arbitrary number of "sectors",* three are indicated in Figure 13 (designated J=1 to 3) each of which is subdivided into an arbitrary number of cells, as illustrated in the figure for sector 2 (J=2) for a 5 radial cell configuration (I=1 to 5). Cell dimensions and distances are expressed in terms of the radial distance r and the polar angle θ, with the origin of coordinates being taken at the corner of the wedge-shaped space.

The outer boundary of the cell system represents the outer limit of the calculated flow region, which is initially specified and moves radially thereafter for each sector according to the speed of the shock wave at the outer boundary of the outermost cell of the sector and the local outer prescribed flow region. The inner and outer boundaries of all cells, such as aa', bb' in Figure 13, are taken to move outward similarly, at speeds proportional to the ratio of their initial radial distances from the origin of coordinates to the initial shock front radius for the same polar angle.

Within each sector the radius from the origin of coordinates to the curved circumferential cell boundaries (aa', etc) is taken to vary linearly with the polar angle between the values at the two rays designating the sector boundaries.

*These shapes are not precisely true sectors in that their outer boundaries deviate slightly from circular arcs.

PRECEDING PAGE BLANK-NOT FILMED

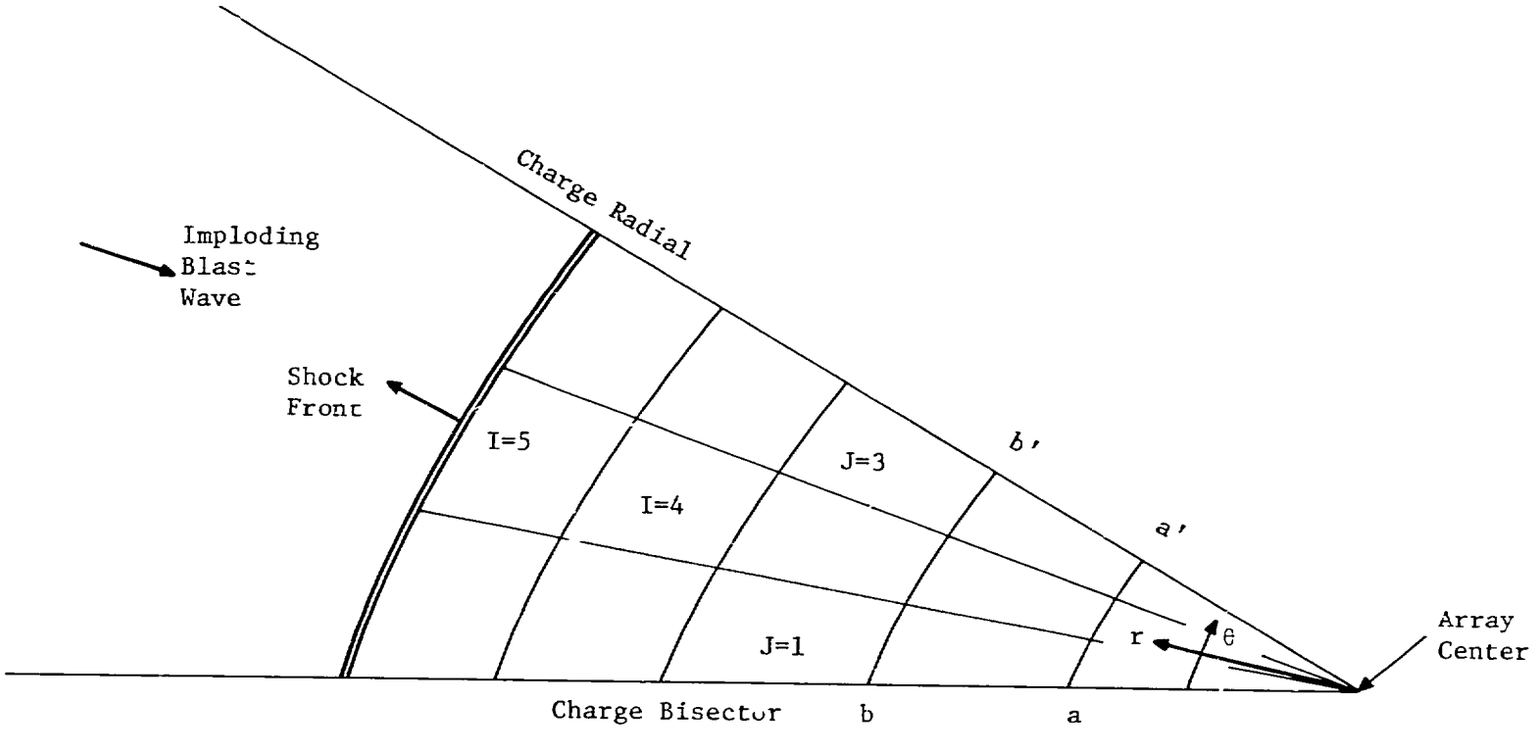

Figure 13. Sketch illustrating the PFAB model.

The pressure, density and velocity components in each cell (abb'a'a, etc.), as expressed in polar coordinates, are taken to be constant throughout the cell.

The flow between adjacent cells in the moving coordinate system is computed using the Godunov technique in the same manner as for the REFLECT-1 code (Reference 2). More specifically, in the interior of the disturbed region, the flux conditions at cell boundaries are computed as locally isentropic shock-expansion phenomena for large pressure and velocity differences between cells, using an isentropic exponent ($\gamma_e = (d\ln(p)/d\ln(\rho))_s$) which is the average of the values for the two adjacent cells; for small pressure and velocity differences between adjacent cells a linearized approximation is used. For the outermost cell boundary of the disturbed region, the shock front velocity and associated fluxes are calculated on the basis of the exact Hugoniot relationships for air.

The code assumes a real air medium with thermodynamic equation-of-state properties given by Brode's 1965 analytical representation (Reference 4).

Input to the code consists of the specification of the pressure, density and velocity in the entire disturbed fluid field at a time shortly before the incident blast wave strikes the corner and also the time dependent incident blast flow conditions outside of the computed flow region for all later times. These required initial and time dependent flow conditions would be obtained from the results of a REFLECT-3 run. The conditions would be inputted to the PFAB code by an interpolation code designated REFRA (Reference 10). The REFRA mating code was developed for use with the REFLECT-1 code. Minor changes are required for its use with the REFLECT-3 code.

Program output consists of tables of pressure, density and velocity and configuration geometry printouts for selected times.

The PFAB code has been set up on a CDC CYBER 176 computer. The code has a core requirement of 164K octal SCM and 376K octal LCM for a 5000 cell configuration.

DISTRIBUTION LIST

DEPARTMENT OF DEFENSE

Assistant to the Secretary of Defense
Atomic Energy
ATTN: Executive Assistant

Defense Advanced Rsch Proj Agency
ATTN: TIO

Defense Intelligence Agency
ATTN: RDS-3A

Defense Nuclear Agency
ATTN: SPSS, J. Galloway
2 cy ATTN: SPSS, G. Ullrich
4 cy ATTN: TITL

Defense Technical Information Center
12 cy ATTN: DD

Field Command
Defense Nuclear Agency
ATTN: FCTMD
ATTN: FCTR

Field Command
Defense Nuclear Agency
Livermore Division
ATTN: FCPRL

Joint Strat Tg Planning Staff
ATTN: NRI, STINFO Library
ATTN: XPFS

Undersecretary of Def for Rsch & Engrg
ATTN: Strategic & Space Systems (OS)

DEPARTMENT OF THE ARMY

BMD Advanced Technology Center
Department of the Army
ATTN: ATC-T

BMD Systems Command
Department of the Army
ATTN: BMDSC-HW

Chief of Engineers
Department of the Army
ATTN: DAEN-ASI-L
ATTN: DAEN-RDL
ATTN: DAEN-MPE-T, D. Reynolds

Harry Diamond Laboratories
Department of the Army
ATTN: DELHD-N-P
ATTN: DELHD-I-TL

U.S. Army Ballistic Research Labs
ATTN: DRDAR-BLT, J. Keefer
ATTN: DRDAR-TSB-S

U.S. Army Cold Region Res Engr Lab
ATTN: Library

U.S. Army Construction Engrg Res Lab
ATTN: Library

DEPARTMENT OF THE ARMY (Continued)

U.S. Army Engineer Center
ATTN: Technical Library

U.S. Army Engr Waterways Exper Station
ATTN: WESSA, W. Flathau
ATTN: WESSD, J. Jackson
ATTN: J. Zelasko
ATTN: Library

U.S. Army Material & Mechanics Rsch Ctr
ATTN: Technical Library

U.S. Army Materiel Dev & Readiness Cmd
ATTN: DRXAM-TL

U.S. Army Nuclear & Chemical Agency
ATTN: Library
ATTN: J. Simms

DEPARTMENT OF THE NAVY

Naval Construction Battalion Center
ATTN: Code L08A
ATTN: Code L51, J. Crawford
ATTN: Code L53, J. Forrest

Naval Postgraduate School
ATTN: Code 0142, Library
ATTN: G. Lindsay

Naval Research Laboratory
ATTN: Code 2627

Naval Surface Weapons Center
ATTN: Code F31
ATTN: Code X211

Naval Surface Weapons Center
ATTN: Tech Lib & Info Svc Br

Office of Naval Research
ATTN: Code 715

DEPARTMENT OF THE AIR FORCE

Air Force Institute of Technology
ATTN: Library

Air Force Systems Command
ATTN: DLWM

Air Force Weapons Laboratory
Air Force Systems Command
ATTN: NTE, M. Plamondon
ATTN: SUL
ATTN: NTV, D. Payton
ATTN: NTED-I
ATTN: NTED-A
ATTN: DEY
ATTN: NTES-S
ATTN: NTES-G
ATTN: NTEO

Assistant Chief of Staff, Intelligence
Department of the Air Force
ATTN: IN

PRECEDING PAGE BLANK-NOT FILMED

DEPARTMENT OF THE AIR FORCE (Continued)

Assistant Secretary of the AF
Rsch, Dev & Logistics
Department of the Air Force
ATTN: SAFALR/DEP for Strat & Space Sys

Ballistic Missile Office
Air Force Systems Command
ATTN: MNNX, W. Crabtree
ATTN: MNNXH, M. Delvecchio
ATTN: MNNXH, D. Gage

Strategic Air Command
Department of the Air Force
ATTN: J. McKinney

Deputy Chief of Staff
Rsch, Dev, & Acq
Department of the Air Force
ATTN: AFRDQI, N. Alexandrow
ATTN: AFRDPN
ATTN: AFRDQA
ATTN: AFRDQI

Strategic Air Command
Department of the Air Force
ATTN: XPFS
ATTN: NRI, STINFO Library

VELA Seismology Center
ATTN: G. Ullrich

DEPARTMENT OF ENERGY CONTRACTORS

Lawrence Livermore National Laboratory
ATTN: D. Glenn

Los Alamos National Scientific Laboratory
ATTN: R. Sanford
ATTN: C. Keller

Sandia National Laboratories
ATTN: A. Chabai
ATTN: Org 1250, W. Brown

OTHER GOVERNMENT AGENCY

Central Intelligence Agency
ATTN: OSWR/NED

DEPARTMENT OF DEFENSE CONTRACTORS

Acurex Corp
ATTN: J. Stockton
ATTN: K. Triebes
ATTN: C. Wolf

Aerospace Corp
ATTN: H. Mirels
ATTN: Technical Information Services

Agbabian Associates
ATTN: M. Agbabian

Applied Theory, Inc
2 cy ATTN: J. Trulio

ARTEC Associates, Inc
ATTN: S. Gill

DEPARTMENT OF DEFENSE CONTRACTORS (Continued)

Boeing Co
ATTN: Aerospace Library
ATTN: S. Strack

California Research & Technology, Inc
ATTN: M. Rosenblatt
ATTN: Library

Civil Systems, Inc
ATTN: G. Melzer

University of Denver
ATTN: J. Wistoski

Eric H. Wang
Civil Engineering Rsch Fac
University of New Mexico
ATTN: J. Kovarna
ATTN: P. Lodde
ATTN: J. Lamb

General Electric Company—TEMPO
ATTN: DASIAC

H-Tech Labs, Inc
ATTN: B. Hartenbaum

Higgins, Auld & Associates
ATTN: J. Bratton
ATTN: N. Higgins
ATTN: H. Auld

IIT Research Institute
ATTN: Documents Library

J. H. Wiggins Co, Inc
ATTN: J. Collins

Kaman AviDyne
ATTN: R. Ruetenik

Merritt CASES, Inc
ATTN: Library

Mission Research Corp
ATTN: G. McCartor
ATTN: C. Longmire

Nathan M. Newmark Consult Eng Svcs
ATTN: N. Newmark
ATTN: W. Hall

Pacific-Sierra Research Corp
ATTN: H. Brode

Pacifica Technology
ATTN: Tech Library

Physics International Co
ATTN: J. Thomsen
ATTN: Technical Library
ATTN: F. Sauer

Science Applications, Inc
ATTN: R. Schlaug
ATTN: H. Wilson
ATTN: Technical Library

DEPARTMENT OF DEFENSE CONTRACTORS (Continued)

R & D Associates
ATTN: R. Port
ATTN: J. Carpenter
ATTN: P. Haas
ATTN: A. Kuhl
ATTN: J. Lewis
ATTN: Technical Info Center
ATTN: C. MacDonald

Science Applications, Inc
ATTN: D. Hove

Science Applications, Inc
ATTN: B. Chambers III
ATTN: W. Layson

SRI International
ATTN: J. Colton
ATTN: D. Johnson
ATTN: G. Abrahamson
ATTN: Library

Systems, Science & Software, Inc
ATTN: K. Pyatt
ATTN: C. Dismukes
ATTN: Library
ATTN: J. Barthel

Systems, Science & Software, Inc
ATTN: C. Needham

DEPARTMENT OF DEFENSE CONTRACTORS (Continued)

Systems, Science & Software, Inc
ATTN: J. Murphy

Systems, Science & Software, Inc
ATTN: C. Hastings

Terra Tek, Inc
ATTN: A. Abou-Sayed
ATTN: Library

TRW Defense & Space Sys Group
ATTN: Technical Information Center
ATTN: N. Lipner
ATTN: T. Mazzola

TRW Defense & Space Sys Group
ATTN: P. Dai
ATTN: E. Wong
ATTN: G. Hulcher

Weidlinger Assoc, Consulting Engineers
ATTN: I. Sandler

Weidlinger Assoc, Consulting Engineers
ATTN: J. Isenberg